ANL/GTRI/TM-13/3

A Description of the Mechanistic DART-THERMAL Dispersion Fuel Performance Code and Application to Irradiation Behavior Analysis of U-Mo/Al

Nuclear Engineering Division

About Argonne National Laboratory

Argonne is a U.S. Department of Energy laboratory managed by UChicago Argonne, LLC under contract DE-AC02-06CH11357. The Laboratory's main facility is outside Chicago, at 9700 South Cass Avenue, Argonne, Illinois 60439. For information about Argonne and its pioneering science and technology programs, see www.anl.gov.

Availability of This Report

This report is available, at no cost, at http://www.osti.gov/bridge. It is also available on paper to the U.S. Department of Energy and its contractors, for a processing fee, from:

U.S. Department of Energy
Office of Scientific and Technical Information
P.O. Box 62
Oak Ridge, TN 37831-0062
phone (865) 576-8401
fax (865) 576-5728
reports@adonis.osti.gov

Disclaimer

This report was prepared as an account of work sponsored by an agency of the United States Government. Neither the United States Government nor any agency thereof, nor UChicago Argonne, LLC, nor any of their employees or officers, makes any warranty, express or implied, or assumes any legal liability or responsibility for the accuracy, completeness, or usefulness of any information, apparatus, product, or process disclosed, or represents that its use would not infringe privately owned rights. Reference herein to any specific commercial product, process, or service by trade name, trademark, manufacturer, or otherwise, does not necessarily constitute or imply its endorsement, recommendation, or favoring by the United States Government or any agency thereof. The views and opinions of document authors expressed herein do not necessarily state or reflect those of the United States Government or any agency thereof, Argonne National Laboratory, or UChicago Argonne, LLC.

ANL/GTRI/TM-13/3

A Description of the Mechanistic DART-THERMAL Dispersion Fuel Performance Code and Application to Irradiation Behavior Analysis of U-Mo/Al

by
B. Ye, J. Rest, and Y.S. Kim
Nuclear Engineering Division, Argonne National Laboratory

March 2013

Nomenclature

AFIP	Advanced Test Reactor Full size plate In center flux trap Position
ANL	Argonne National Laboratory
ATR	Advanced Test Reactor
DART	Dispersion Analysis Research Tool
DART-THERMAL	Dispersion Analysis Research Tool coupled with a temperature calculation subroutine
IL	Interaction Layer or Interdiffusion Layer
INL	Idaho National Laboratory
OM	Optical Microscopy
PIE	Post Irradiation Examination
RERTR	Reduced Enrichment for Research and Test Reactors
SEM	Scanning Electron Microscopy

Table of Contents

NOMENCLATURE ..... **II**

SECTION 1 ..... **1**

INTRODUCTION **1**

SECTION 2 ..... **3**

FUEL MEAT THERMAL DEGRADATION OF DISPERSION FUELS IRRADIATION **3**

2.1 INTERACTION LAYER GROWTH EFFECT 3
2.2 FISSION GAS BUBBLE FORMATION IN U-MO PARTICLES 4
2.3 MATRIX PORE FORMATION 5

SECTION 3 ..... **6**

FISSION GAS BEHAVIOR MODELING **6**

SECTION 4 ..... **13**

FUEL MEAT SWELLING **13**

4.1 INTERACTION LAYER GROWTH 13
4.1.1 Interaction layer growth correlation for U-Mo/Al fuels *13*
4.1.2 Interaction layer growth correlation for U_3Si_2 fuels *14*
4.2 FUEL MEAT SWELLING 14

SECTION 5 ..... **17**

THERMAL MODEL IN DART-THERMAL **17**

5.1 COOLANT TEMPERATURE CALCULATION 18
5.2 OXIDATION LAYER SURFACE TEMPERATURE 19
5.3 OXIDATION LAYER-CLADDING INTERFACE TEMPERATURE 20
5.4 CLADDING-FUEL MEAT INTERFACE TEMPERATURE 20
5.5 FUEL MEAT TEMPERATURE 20

SECTION 6 ..... **22**

MODEL VALIDATION AGAINST RERTR-5 EXPERIMENTAL DATA **22**

6.1 OPERATIONAL CONDITIONS AND FUEL FABRICATION PARAMETERS 22
6.2 RESULTS AND DISCUSSION 23

SECTION 7 ..... **27**

VALIDATION AGAINST RERTR-6, 7, 9 TEST DATA **27**

7.1 OPERATIONAL CONDITIONS AND FUEL FABRICATION PARAMETERS 27
7.2 RESULTS AND DISCUSSION 27

SECTION 8 ..... **31**

AFIP-1 FULL-SIZED PLATE TEST **31**

8.1 EXPERIMENT DESCRIPTION 31
8.2 POWER HISTORY AND COOLANT TEMPERATURE 33

8.3 RESULTS AND DISCUSSION 35

SECTION 9 39

PROPOSED APPLICATION OF U_3SI_2/AL DISPERSION FUEL IN RHF 39

9.1 PARAMETERS APPLIED IN THE CALCULATIONS FOR RHF FUEL 39
9.2 CALCULATION RESULTS 40

SECTION 10 42

SUMMARY AND FUTURE WORK 42

REFERENCES 44

APPENDIX I. DART-THERMAL INPUT DESCRIPTION 47

APPENDIX II. DART-THERMAL OUTPUT DESCRIPTION 55

APPENDIX III. DART-THERMAL INSTALLATION DESCRIPTION 57

III.1 FILES REQUIRED TO INSTALL DART-THERMAL 57
III.2 DART-THERMAL INSTALLATION INSTRUCTIONS 57

Section 1

Introduction

Dispersion Analysis Research Tool (DART) and DART-THERMAL are thermomechanical models developed for integrated fuel performance modeling [1-5]. These models calculate irradiation-induced swelling as a function of fuel morphology, and the macroscopic changes in rod diameter or plate/tube thickness due to fuel swelling processes. Moreover, the codes follow fuel restructuring due to aluminum-fuel reaction, amorphization, and recrystallization during fuel irradiation. These comprehensive models were designed to predict fuel behavior from a fundamental and theoretical approach by integrating multiple physical and mechanical mechanisms.

DART-THERMAL was developed based on DART [3-5]. DART-THERMAL includes the same features for predicting irradiation-induced-swelling behavior of dispersion fuel as DART, but incorporates a one-dimensional heat transfer model that is integrated with the mechanical and swelling analyses. At each time step, temperature distributions across the fuel element are calculated based on power density, coolant temperature, and meat thermal conductivity. Subsequently, swelling of solid fission products and of fission gas bubbles in each fuel region is calculated, as well as the interaction between the U-Mo fuel particles and the matrix Al. The behavior of fission gas in the amorphous interaction product is also considered. At the same time, commensurate changes in the constituent volume fractions, and associated changes in thermal conductivity and hydrostatic stress are calculated.

A detailed report about the thermomechanical model DART for the prediction of fission-product-induced swelling in aluminum dispersion fuel was published in 1995 [1]. Physical models for the prediction of fission-product-induced swelling in Al dispersion fuels, and analysis results for U_3Si and U_3Si_2 dispersion fuels were described in [1]. Since then, the DART code has been continuously developed in order to improve its capabilities in predicting macroscopic fuel performance. One of the significant improvements was addition of a 1-D thermal analysis model, which made possible the simulation of the strong interrelationship between fuel temperature and fuel-matrix interaction [3-5]. A user-friendly graphic interface was introduced in DART-THERMAL to facilitate a user-friendly environment. Other improvements include the recent implementation of interaction layer growth correlations with Si addition, a modified constituent volume fraction calculation approach, an equal thickness fuel particle nodalization method, updated oxide growth correlations and optimized materials properties for fission gas bubble behavior, etc [6-8].

This report describes the primary physical models that form the basis of the DART-THERMAL mechanistic computation code for calculating swelling of Al dispersion fuels during irradiation. Since some of the theoretic models were elaborated in [1], this report will place the emphases on the models related to the recent improvements. Model validation is demonstrated by comparing with experimental data for U-Mo/Al dispersion fuels. Interaction layer growth, meat constituent volume fractions, fuel

meat swelling, and inter-granular gas bubble size distributions are calculated and compared to data obtained from RERTR tests in the Advanced Test Reactor (ATR). DART-THERMAL input instructions, and output file description are provided in the appendixes.

Section 2

Fuel Meat Thermal Degradation of Dispersion Fuels Irradiation

Accurate calculation of fuel element temperature is critical to fuel performance modeling, and it is essentially dependent on the correct estimation of fuel meat thermal conductivity, which in turn, is influenced by local fuel morphology and material chemical composition. There are three major factors degrading thermal conductivity of the fuel meat: interaction layer growth between fuel particles and Al matrix, fission gas bubble formation in fuel particles, and pore formation outside fuel particles. All of these factors are considered in the thermal conductivity calculations in DART-THERMAL. In order to estimate the effective fuel thermal conductivity, fuel meat is considered as a multiphase material, consisting of unreacted fuel, Al matrix, porosity, and interaction layer.

2.1 Interaction layer growth effect

As the irradiation proceeds, the interaction layer between Al matrix and fuel particles grows thicker, and the resultant low-conductivity reaction product greatly hinders fission-generated heat from flowing into the matrix. Consequently, the correct fuel thermal conductivity can only be obtained by an accurate description of volume changes associated with each meat component. In turn, the thermal conductivity controls interaction layer growth through its effect on heat transfer. The calculation of fuel deformation and thermal conductivity is interactive with the thermal analysis throughout the calculation.

A multiphase thermal conductivity model is employed in DART-THERMAL to calculate effective fuel thermal conductivity [9]. The effective fuel thermal conductivity is represented as:

$$k_{meat0} = \frac{1}{4}[A + (A^2 + 8\,fm)^{1/2}] \qquad (2.1)$$

$$A = -f + 3Vf + 2m - 3Vm \qquad (2.2)$$

where k_{meat0} is the effective thermal conductivity of the fuel meat without porosity, *f* is the composite thermal conductivity of the fuel and reaction-product phase, *m* is the thermal conductivity of aluminium, and *V* is the volume fraction of the fuel particle together with interaction layer. A value of m = 225 W/(m·K) is used here for the aluminum thermal conductivity, and *V* evolves due to the irradiation-induced change in microstructure and chemical compositions. The accurate modeling of *f* is described in [9] and summarized below.

The composite thermal conductivity of the fuel and reaction-product phase *f* is calculated by taking into account the thermal conductivities of unreacted fuel (k^{g}_{U-Mo}) and reaction products ($k_{UAl\ln}$) as described in Eqn. (2.3) [9].

$$f = \frac{1}{\dfrac{r_{sf} - y_{IL}}{r_{sf} \bullet k^{g}_{U-Mo}} + \dfrac{y_{IL}}{r_{sf} \bullet k_{UAl\ln}}} \qquad (2.3)$$

where k^{g}_{U-Mo} is the unreacted U-Mo fuel thermal conductivity in W/(m·K); k_{UAl_3} = 3.0 W/(m·K) is the thermal conductivity of reaction-product phase; and r_{sf} and y_{IL} are the fuel particle radius and interaction layer thickness in m respectively.

The unreacted U-Mo fuel thermal conductivity k^{g}_{U-Mo} is derived based on the thermal conductivity of unirradiated U-Mo fuel k^{0}_{U-Mo} with an additional correction for fission gas bubbles in fuel particles. The thermal conductivity of unirradiated U-Mo fuel is given by

$$k^{0}_{U-Mo} = (1-\sqrt{1-x_{Mo}})k_{Mo} + \sqrt{1-x_{Mo}}\{(1-x_{Mo})k_U + x_{Mo}k_{c,Mo}\} \quad (2.4)$$

and is derived by fitting the available measurement data for U-Mo alloys [9]. Here k^{0}_{U-Mo} is in W/(m·K), x_{Mo} is the Mo content in weight fraction. k_U and k_{Mo} represent the thermal conductivities in W/(m·K) of uranium and molybdenum metals respectively, and are given by

$$k_U(T) = 21.73 + 1.591\times10^{-2}T + 5.907\times10^{-6}T^2 \quad (2.5)$$

$$k_{Mo}(T) = 150.0 - 4.0\times10^{-2}T \quad (2.6)$$

where T is the temperature in K.

2.2 Fission gas bubble formation in U-Mo particles

Porosity is also accounted for in the fuel meat thermal conductivity calculation. There are three classes of porosity observed in fuel plates: small gas bubbles generated within fuel particles and within interaction layers, large pores residing in the Al matrix, which include the as-fabricated pores, and the fission-gas-filled pores located at the particle-matrix interface. All three types of porosity can effectively reduce fuel meat thermal conductivity, but only the first two types of porosity are considered in the model. The bubbles lying at the particle-matrix interfaces will be incorporated into the model in the future.

The analytical treatment of fission gas bubbles was adapted from the model developed for U_3Si_2 fuel and elaborated in Rest's paper [10]. According to the theoretic analysis, pore geometry and physical properties are of great importance in modeling the thermal conductivity of materials containing pores. Pore geometry is defined by pore size, shape, and orientation with respect to the direction of heat flow; and the related physical properties include the emissivity of the pore surface and the thermal conductivity of the gas trapped within the pore. Therefore, the effective thermal conductivity of fuel particles that contain fission gas k^{g}_{U-Mo} is expressed as follow:

$$k^{g}_{U-Mo} = k^{0}_{U-Mo} + \pi[\frac{k_g}{2}(R_g/l_g) - k^{0}_{U-Mo}(R_g/l_g)^2] \quad (2.7)$$

where k_{U-Mo}^{g} and k_{U-Mo}^{0} are in W/(m·K); R_g and l_g are mean bubble radius in cm and interbubble spacing in cm, respectively; k_g in W/(m·K) is the fission gas thermal conductivity. By assuming Xe is the major component, k_g can be expressed as

$$k_g = 4.0288 \times 10^{-5} T^{0.872} \tag{2.8}$$

where *T* is temperature in K. R_g and l_g are calculated at each time step with the mechanistic fission gas behavior model in DART-THERMAL.

2.3 Matrix pore formation

The impact of large matrix pores on fuel meat thermal conductivity is taken into account by applying a correction factor on k_{meat0}. The final form of effective fuel meat thermal conductivity is given by:

$$k_{meat} = k_{meat0} f(P) \tag{2.9}$$

where $f(P)$ is a correction factor for porosity in the Al matrix. It is defined in Eqn. (2.10) [11]:

$$\begin{aligned} f(P) &= \exp(-2.14P) && 0.0 \le P \le 0.30 \\ &= 0.92 - 1.34P && 0.3 < P \le 0.5 \end{aligned} \tag{2.10}$$

where *P* is the volume fraction of porosity. The porosity *P* includes the as-fabricated pores.

Section 3

Fission Gas Behavior Modeling

Fission gases produced in nuclear fuels during irradiation can have a great impact on fuel performance. The inert fission gases (Xe, Kr) are known to precipitate into gas bubbles due to their extremely low solubility in the fuel matrix. The bubbles grow by absorbing gas atoms generated as a by-product of the fission reactions, and by coalescing with each other. The resultant growth of bubbles can then lead to appreciable fuel swelling.

Fission-gas-driven swelling is one of the major components in U-Mo/Al dispersion fuel meat swelling. Fission gases reside in solution, as small intragranular (within fuel grains) bubbles, and as relatively large intergranular (between fuel grains) bubbles. The accumulation of gas atoms on grain boundaries can account for an appreciable component of the fuel swelling. Hence modeling of the intergranular gas bubble formation and growth, and prediction of the number density and size of these bubbles is of great importance in predicting fuel swelling. In addition, the shape of the bubble-size distribution reveals the nature of the behavioral mechanisms which are not exhibited in average bubble size calculations [12, 13].

The fission gas behavior model in DART-THERMAL is based on the mechanistic Steady-State and Transient-Gas Release and Swelling Subroutine (GRASS-SST) [14]. Mechanisms for various fission gas phenomena, such as fission product generation, atomic migration, bubble nucleation and re-solution, bubble migration, and coalescence, are postulated based on theoretical and/or experimental observation and are expressed mathematically. Fission-gas induced swelling is obtained by the numerical solution of a set of coupled nonlinear differential equations for the intra- and intergranular concentrations of fission-product atoms and gas bubbles. This approach is based on a mechanistic understanding of the physics underlying the experimental observation. In contrast to empirical correlations, it is possible to predict fission gas behavior and its contribution to fuel meat swelling outside the validation database, giving that the related materials properties are available. These equations are of the form

$$\frac{dC_i^\alpha}{dt} = -a_i^\alpha C_i^\alpha C_i^\alpha - b_i^\alpha C_i^\alpha + e_i^\alpha \qquad (I = 1, \ldots, N;\ \alpha = 1, 2, 3, 4) \tag{3.1}$$

where i is the number of atoms in a bubble; C_i^α is the number density of α-type bubbles in the ith-size class; α = 1, 2, 3, 4 represents the location of the bubbles at the lattice, dislocation, grain-face, and grain-edge, respectively; and the coefficients a_i^α, b_i^α, and e_i^α obey functional relationships of the form

$$a_i^\alpha = a_i^\alpha(C_i^\beta)$$

and

$$b_i^\alpha = b_i^\alpha(C_1^\beta,...,C_{i-1}^\beta,C_{i+1}^\beta,...,C_N^\beta)\,. \tag{3.2}$$

The coefficient a_i^α represents the rate at which α-type bubbles are lost from the i th-size class because of coalescence with bubbles in that class; b_i^α represents the rate at which α-type bubbles are lost from the i th-size class because of coalescence with bubbles in other size classes, migration out of the structural region, change in bubble type due to bubble migration processes and re-solution; and e_i^α represents the rate at which bubbles are being added to the i th-size class because of fission gas generation, bubble nucleation, and bubble growth that is a result of bubble coalescence, migration processes, and bubble shrinkage due to gas atom re-solution [14]. The events represented by each term in Eqn. (3.1) are described in Table 3.1.

Table 3.1 Definition of variables in Eqn. (3.1) [14]

A	i	C_i^α	$a_i^\alpha C_i^\alpha C_i^\alpha$	$b_i^\alpha C_i^\alpha$	e_i^α
1,2	1	Concentration of gas atoms in lattice (α = 1) and on dislocations (α = 2)	Rate of gas atom loss due to gas bubble nucleation	Rate of gas atom loss due to diffusive flow to grain boundaries, grain boundary sweeping, and diffusion into gas bubbles	Rate of gas atom gain due to atom re-solution and fission of uranium nuclei
1,2	2,…,N	Concentration of gas bubbles in lattice (α = 1) and on dislocations (α = 2)	Rate of gas bubble loss due to bubble coalescence with bubbles within the same size class	Rate of gas bubble loss due to coalescence with bubbles in other size classes, diffusive flow to grain boundaries (α = 1), grain boundary sweeping, and gas atom re-solution	Rate of gas bubble gain due to bubble nucleation and coalescence, and diffusion of gas atoms into bubbles
3	1,…,N	Concentration of grain-face gas atoms (i = 1) and gas bubbles (i > 1)	Rate of gas bubble loss due to gas bubble nucleation (i = 1) and bubble coalescence with bubbles within the same size class (i > 1)	Rate of gas bubble loss due to coalescence with bubbles in other size classes, venting to grain edges due to grain-face bubble interconnection, and venting of gas to grain corners due to microcracking	Rate of gas bubble gain due to bubble nucleation and coalescence, diffusion of gas atoms into bubbles, and intra-granular migration to grain faces
4	1,…,N	Concentration of grain-edge gas atoms (i = 1) and	Rate of gas bubble loss due to gas bubble nucleation (i	Rate of gas bubble loss due to coalescence with	Rate of gas bubble gain due to bubble nucleation and

		gas bubbles (i > 1)	= 1) and bubble coalescence with bubbles within the same size class (i > 1)	bubbles in other size classes and venting of gas to grain corners due to long-range grain-edge bubble interconnection and microcracking	coalescence, diffusion of gas atoms into bubbles, and the venting of gas from the grain faces

By using the form of Eqn. (3.1) for the change of bubble density in each size class, not only can the evolution of total bubble density and average bubble size be calculated, but also the bubble size distributions at various locations in the fuel can be obtained. In the calculation, within each size class the bubbles are classified by the average number of gas atoms per bubble. Namely, a 1st-size class bubble is a bubble that consists of a single gas atom associated with one or more vacancies, and the i th-size class contains all bubbles with the number of gas atoms in the range of (m (i -1)) to (m i), where m is an integer multiplier (2 ≤ m ≤ 10). This method of bubble grouping significantly reduces the number of equations needed to describe the bubble size distribution.

Essential materials properties, such as the probabilities for bubble nucleation, coalescence and re-solution during irradiation, and bubble diffusivities are dependent upon fuel composition, fuel type, fabrication process, fission rate, and temperature. Some of these parameters are available from experimental measurement, but others have to be derived from theoretic models. Details for deriving a_i^α, b_i^α, and e_i^α can be found in [14].

The gas-driven swelling behavior in U-Mo fuels is primarily intragranular at high temperature. However, at low temperature (≤ 200°C), intergranular swelling becomes appreciable [13]. Since most of research reactors in the world operate in a temperature range of 100 - 200°C, it is of great importance to understand intergranular gas bubble behavior in order to assess gas-driven fuel swelling safety margins for RERTR program application.

Early results of scoping studies with DART-THERMAL demonstrated that reasonable agreement with measured bubble size distributions in RERTR fuel plates could not be achieved without taking some physical parameters to unrealistic values [15]. Subsequently, this discrepancy was traced to the absence in DART-THERMAL of two relatively new physical mechanisms underlying gas-bubble behavior in U-Mo: multiatom nucleation and sputtering coalescence [13]. These new models have not yet been implemented in the version of DART-THERMAL described in this report. In the interim, values for several physical parameters and materials properties have been adjusted in order to achieve the best agreement with experimental measurements. A brief description of these two mechanisms and the parameter adjustment methodology is given below.

(1) Multi-atom nucleation mechanism

The classic theory of gas bubble nucleation assumes a di-atom nucleation mechanism, in which the nucleation process is continuous throughout the irradiation: a gas bubble nucleus forms whenever two gas atoms join together. In theory, the nucleation process continues until the rate at which newly generated gas atoms form new gas bubbles reaches equilibrium with the rate at which gas atoms join with existing bubbles. Rest proposed a multi-atom nucleation mechanism in [13]. This alternative mechanism treats the nucleation process not by atom-to-atom growth, but by simultaneous gas bubble nucleation. That occurs after initial incubation period, when the gas concentration reaches the solubility limit in the fuel. Subsequently, nucleation is limited, because the gas concentration in solution falls below the solubility limit. The nucleation event repeats when the gas in solution again reaches the solubility limit. Thus, there is an incubation period between subsequent nucleation events. As such, the nucleation factor for intergranular bubbles in the basic model needs to be reduced in order to take into account these incubation phases.

(2) Sputtering coalescence mechanism

Bubble coalescence processes are driven by a random volume diffusion mechanism and/or by the biased motion within a temperature gradient. These two mechanisms have been implemented in the basic DART model, as described in [1]. Both processes involve bubble motion which is limited for larger bubbles and/or at relatively low temperature/temperature gradients. Therefore, sputtering coalescence, or bubble coalescence without bubble motion, is proposed based on implantation studies in pure metals [16]. This process can be understood on the basis of the difference in the probability for an atom to be knocked out of the volume between a pair of bubbles and the probability of an atom to be injected into this inter-bubble volume [13]. The inter-bubble materials are sputtered because of fission damage, and the majority of the sputtered atoms is injected into the adjacent bubbles, with the commensurate drawing together of the bubbles until the joining process has been completed. The sputtering coalescence mechanism has not yet been implemented into DART-THERMAL, and, thus, it might be one of the reasons behind the discrepancy between calculated and measured intergranular bubble size distributions. The enhancement factor for gas atom diffusion on grain boundaries and some related parameters have been adjusted in this study in order to simulate this low-temperature intergranular bubble growth mechanism.

The mechanistic fission-gas-behavior models in DART-THERMAL simulate gas related phenomena in the form of a series of rate theory equations. The confidence level on how realistic the physical models can simulate fission gas behavior is correlated to the accuracy of values of key materials properties. One of the major challenges in the field of fission gas behavior modeling is the determination of key materials properties and behavioral models. The practice of validation against experimental measurement is an indispensable step toward identifying and improving gas behavioral models and/or materials properties.

Since the bubble size distribution contains much more information on the nature of behavioral mechanisms than typically utilized mean values, a close comparison between the predicted and measured bubble size distribution provides a much higher degree of validation than usually found in the

literature. Here the measured intergranular bubble size distributions in UMo/Al dispersion fuels were studied. They were measured from the mini-plates irradiated in the Advanced Test Reactor (ATR) at the Idaho National Laboratory (INL). Intergranular bubbles form at the contact plane of two neighboring fuel grains. Compared to intragranular bubbles which occur inside fuel grains, these bubbles are bigger in size and normally have lenticular shape. At low irradiation temperatures, intergranular bubbles produce an appreciable contribution to the overall swelling of the fuel meat.

In the current study, some of the materials properties used in the rate theory equations are estimated from the literature, and others are still undetermined due to the lack of measurement data. Therefore, a parametric study was performed in order to examine the sensitivity of calculated intergranular bubble size distribution to the related parameter values. From the sensitivity study results, the materials properties that have the most influence on inter-granular bubble size distributions were determined. Furthermore, the values of these materials properties related to fission gas behavior were predicted by adjusting the parameters to achieve the best agreement with the experimental data for V6018G plate (RERTR-5). The parameters and their optimized values are listed in Table 3.2. In the calculations for the other two fuel plates, V6019G and V8005H, the same parameters were applied.

Table 3.2 Values of optimized parameters used in the calculations

Parameter	Symbol	Unit	Value
Resolution rate	$b_0 (b = b_0 \dot{f})$	cm^3	$3x10^{-18}$
Gas atom diffusivity	$D_0 (D_g = D_0 \dot{f})$	cm^5/s	$2x10^{-27}$
Bubble nucleation factor on grain boundaries	f_n	N/A	$6x10^{-7}$
Fuel surface energy	γ	J/m^2	0.2
Enhancement factor for gas atom irradiation-enhanced diffusion on grain boundaries	ξ	N/A	$1x10^4$
Activation energy for gas atom diffusion	Q	cal	33000

The intergranular bubble size distributions calculated for V6018G, V6019G and V8005H are shown in Figure 3.1-3.3 respectively. They agree reasonably well with the experimental data. The slight deviation from the experimental data can be eliminated by introducing additional gas behavioral mechanisms, such as multi-atom nucleation and sputtering coalescence on grain boundaries [13].

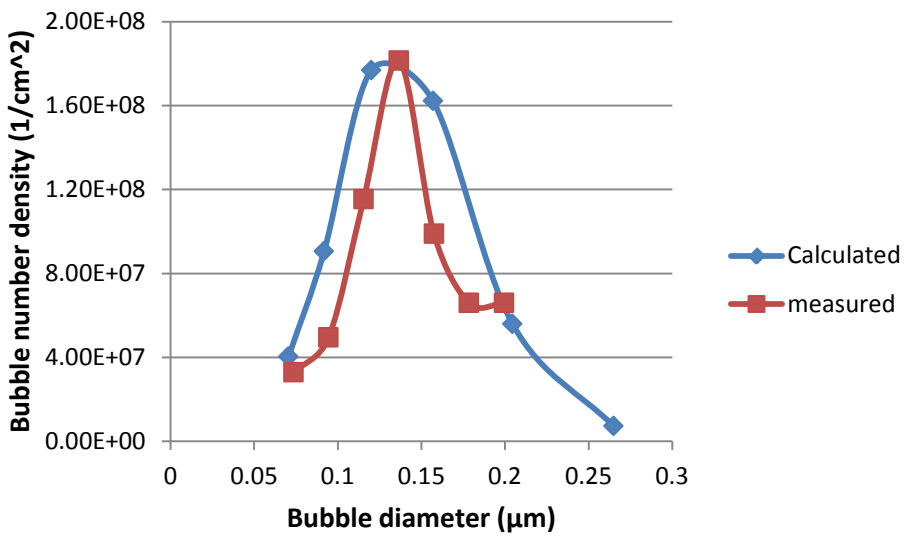

Figure 3.1 Comparison of predicted and measured intergranular bubble size distributions for V6018G

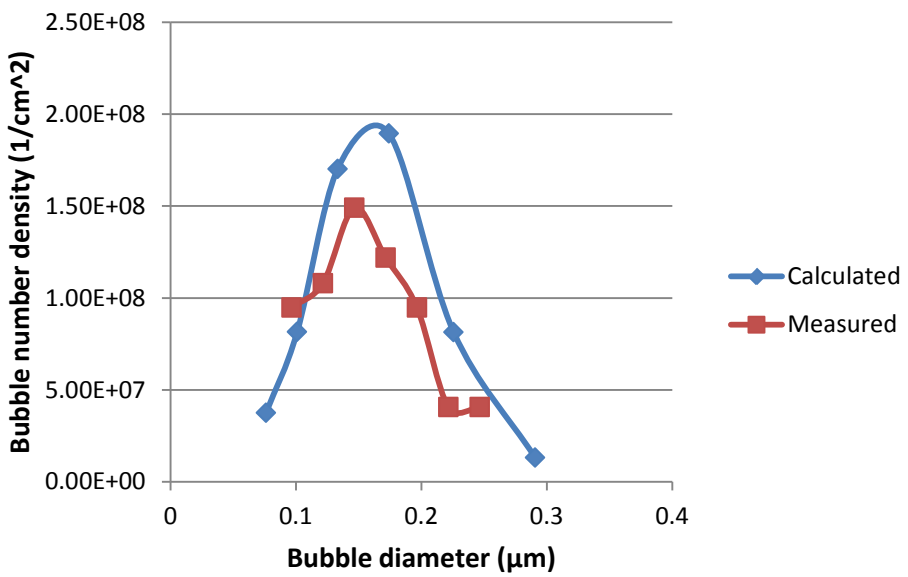

Figure 3.2 Comparison of predicted and measured intergranular bubble size distributions for V6019G

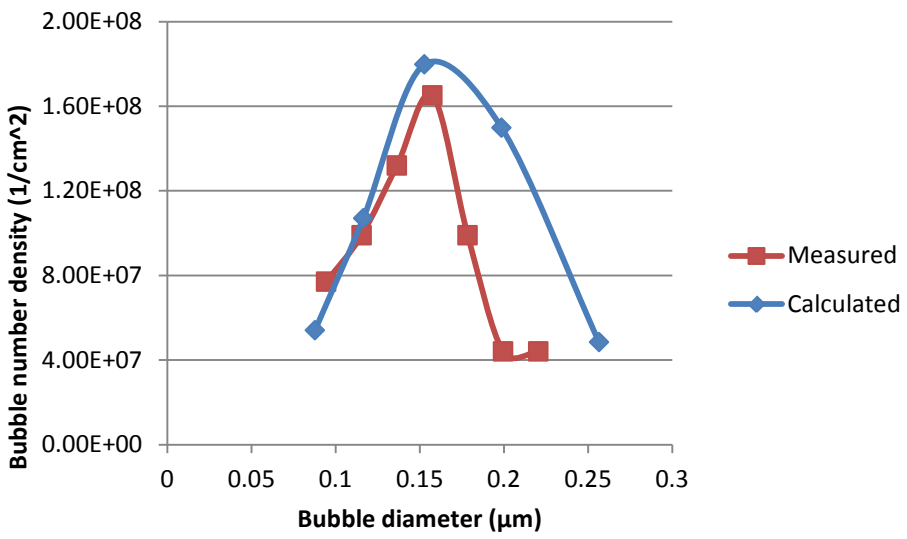

Figure 3.3 Comparison of predicted and measured intergranular bubble size distributions for V8005H

Section 4

Fuel Meat Swelling

Fuel meat swelling in UMo/Al dispersion fuel is a combined effect resulting from the accumulation of fission product elements and fuel microstructural changes which include the formation of an interaction layer and irradiation-enhanced sintering of fabrication voids. Fission-product-induced swelling consists of two parts: one part comes from solid fission products which have different atomic volumes from fissioned uranium atoms, and the other part is caused by fission gas bubble formation.

4.1 Interaction layer growth

4.1.1 Interaction layer growth correlation for U-Mo/Al fuels

The interaction layer (IL) growth correlation employed in DART-THERMAL was developed primarily by using mini-plate test data with/without Si addition in the Al matrix [17]. It can be applied to fuels having Si content between 0 – 8 wt.% in the matrix, and temperatures between 90 – 200 °C. The correlation is expressed below (Eqn. (4.1)), by multiplying the correlation for the samples with a pure Al matrix (Eqn. (4.2)) with additional factors for Si addition in the matrix and Mo content in the U-Mo alloy:

$$Y_i^2 = Y_{i,0}^2 f_{Si} f_{Mo} \tag{4.1}$$

Y_i is the IL thickness, and $Y_{i,0}$ represents the IL thickness in a sample without Si addition in the matrix. f_{Si} and f_{Mo} are the factors for Si-addition and Mo content respectively. Detailed descriptions of $Y_{i,0}$, f_{Si}, and f_{Mo} are as follows.

$$Y_{i,0}^2 = 2.6\times10^{-16}\,\dot{f}^{\,0.5}\exp(-\frac{3850}{T})t \tag{4.2}$$

Here $Y_{i,0}$ is in cm, $\dot{f}$ is the fission rate in f/cm^3-s. T is the fuel temperature in K, and t is irradiation time in s.

The addition of Si in the Al matrix can reduce IL thickness significantly. Its effect on IL growth also depends on temperature, as shown by the factor f_{Si}:

$$\begin{aligned} f_{Si} &= [0.97 - 0.00062(T-373)]\exp[-(2.5-0.021(T-373))W_{Si}] \\ &+ [0.026 + 0.00062(T-373)]\exp[-(0.00081(T-373))W_{Si}] \end{aligned} \tag{4.3}$$

Where T is the fuel temperature in K (< 200 °C), and W_{Si} is the Si content in the matrix in weight % (< 8 wt.%).

According to the PIE analyses on mini-plate fuels, the IL growth decreases when the Mo content in U-Mo alloy increases. For the fuel plates with various Mo contents, a Mo content factor is formulated such that the IL growth rate decreases linearly with the Mo content in the range of 6-10 wt.%.

$$f_{Mo} = 1.35 - 0.05W_{Mo} \quad (4.4)$$

Where W_{Mo} is the Mo content in fuel particles in wt.%.

4.1.2 Interaction layer growth correlation for U_3Si_2 fuels

DART-THERMAL model for aluminum silicide fuel reaction is established using the correlation for interdiffusion layer (IL) between U_3Si_2 and Al. The correlation used in this analysis is the ANL correlation developed from in-pile test data [18], which is given as below:

$$Y^2 = A_{irr} \exp(-\frac{Q_{irr}}{RT}) \dot{f}^{0.5} t \quad (4.5)$$

where Y the IL thickness in µm, A_{irr}= 2.2x10^{-8}, Q_{irr}= 40.6 kJ/mol, R = 1.985x10^{-3} kJ/mol-K the gas constant, T the fuel temperature in K, $\dot{f}$ the fission rate in fission/(cm^{3}s), and t the total irradiation time in s.

4.2 Fuel meat swelling

The swelling contribution from solid fission products is caused by volume difference between fissioned uranium atoms and solid fission products; therefore this type of swelling is strongly dependent on the fission density. In DART-THERMAL, this component of swelling is modeled using an empirical equation derived based on PIE data from RERTR tests, which is given by:

$$(\frac{\Delta V}{V_0})_s = 4.0 f_d \quad (4.6)$$

where $(\frac{\Delta V}{V_0})_s$ is the fuel swelling caused by solid fission products in %, and f_d is fission density in 10^{27} fissions/m^3 [18].

Another important source of fuel swelling is from fission gases. PIE micrographs have shown that many SEM observable gas bubbles aggregate along grain boundaries in UMo fuels. The fission-gas-driven fuel swelling is calculated through the complex models described in Section 3. The fission-gas-induced swelling $(\frac{\Delta V}{V_0})_g$ consists of fuel swelling induced by gas bubbles located in the lattice and on grain boundaries. Both fuel and interaction layer are subject to the swelling caused by solid and gaseous fission products.

Aside from fission-product-swelling, depletion of high-density UMo fuel (17.2 g/cm^3) and accumulation of low-density reaction product $(U_aMo_{1-a})Al_x$ (4-5 g/cm^3) play a major role in UMo/Al dispersion fuel swelling. This volume change can be calculated as:

$$(\frac{\Delta V}{V_0})_{RP} = \frac{Mw_{RP}}{d_{RP}} \Big/ \frac{Mw_{UMo}}{d_{UMo}} - 1 \quad (4.7)$$

here $(\frac{\Delta V}{V_0})_{RP}$ is the meat volume change due to reaction product formation; Mw_{RP} and Mw_{UMo} are the molecular weights of reaction product and alloy fuel respectively, and d_{RP} and d_{UMo} are their respective densities. PIE compositional analyses show that the stoichiometry of reaction product $(U_aMo_{1-a})Al_x$ changes with burnup, where x varies within a range of 3 – 7. As an example, assume the reaction product is in a form of $(U_aMo_{1-a})Al_7$ (the molecular weight and density are listed in Table 4.1), then the reacted fuel volume increases 5.65 times with respect to its unreacted form.

Table 4.1 Molecular weight and density of reaction products and UMo alloy

	Molecular weight Mw (g/mol)	Density d (g/cm^3)
$(U_aMo_{1-a})Al_5$	390.4	5.17
$(U_aMo_{1-a})Al_7$	444.4	5.14
$U_{0.9}Mo_{0.1}$	255.4	17.2

The last component of meat volume change is caused by irradiation-enhanced sintering ($(\frac{\Delta V}{V_0})_{porosity}$). During the fabrication process, voids and microcracks are left in the dispersion fuel meat. These porosities help to accommodate fission products and to eliminate fuel volume increase during reactor operation. Once the as-fabricated pores are sintered shut, the fuel meat starts to swell.

It needs to be pointed out that the model in DART-THERMAL neglects Al matrix swelling during reactor operation. This assumption is based on the fact that the Al matrix has a much smaller swelling rate as compared to fuel particles. Thus, the total fuel meat swelling is the summation of meat volume changes induced by IL formation, accumulation of fission product elements, and irradiation-enhanced sintering.

Fuel meat swelling calculation starts with the total fuel particle swelling. Eqns. (4.8) and (4.9) show the total fuel particle swelling calculation at each time step.

$$\begin{aligned} V_{fuel} &= V_{fuel}^0 \times (1 - f_{reacted}) \times (1 + (\frac{\Delta V}{V_0})_s + (\frac{\Delta V}{V_0})_g) \\ &+ V_{fuel}^0 \times f_{reacted} \times (1 + (\frac{\Delta V}{V_0})_{RP}) \times (1 + (\frac{\Delta V}{V_0})_s + (\frac{\Delta V}{V_0})_g) \end{aligned} \tag{4.8}$$

$$(\frac{\Delta V}{V_0})_{fuel} = \frac{V_{fuel} - V_{fuel}^0}{V_{fuel}^0} \tag{4.9}$$

Here $(\frac{\Delta V}{V_0})_{fuel}$ represents the total fuel particle swelling; V_{fuel}^0 and V_{fuel} are volumes of the total fuel particles before and after irradiation, respectively; $(\frac{\Delta V}{V_0})_s$, $(\frac{\Delta V}{V_0})_g$, and $(\frac{\Delta V}{V_0})_{RP}$ are volume changes

of fuel particles caused by solid fission products, gaseous fission products, and interaction layer formation, respectively; $f_{reacted}$ is the volume fraction of reacted fuel, which can be derived from the IL thickness.

The Al matrix volume change needs to be taken into account in order to convert the fuel particle swelling into fuel meat swelling. Eqn. (4.10) is used to calculate the initial Al volume V_{Al}^{0}.

$$V_{Al}^{0} = V_{fuel}^{0}\left(\frac{1-p_{fuel}^{0}}{p_{fuel}^{0}}\right) \tag{4.10}$$

where $p_{fuel}^{0} = V_{fuel}^{0} / V_{meat}^{0}$ is the initial fuel volume fraction in the fresh fuel. Since the Al matrix is continuously consumed by reacting with U-Mo fuel during irradiation, the Al volume after irradiation is calculated in Eqn. (4.11).

$$V_{Al} = V_{Al}^{0} - (V_{fuel}^{0} \times f_{reacted}) \times x \times \frac{Mw_{Al}}{d_{Al}} / \frac{Mw_{RP}}{d_{RP}} \tag{4.11}$$

where x is the Al stoichiometry in $(U_aMo_{1-a})Al_x$; Mw_{Al} is the molecular weight of Al, which is 27 g/mol, and d_{Al} =2.7 g/cm^3 is the density of Al.

The total volume of fuel meat after irradiation can be calculated based on Eqns. (4.8) and (4.11):

$$V_{meat} = (V_{fuel} + V_{Al}) \times \left(1 - \left(\frac{\Delta V}{V_0}\right)_{porosity}\right) \tag{4.12}$$

In Eqn. (4.12), the minus sign in front of $\left(\frac{\Delta V}{V_0}\right)_{porosity}$ is derived from the irradiation-induced sintering effect. Finally, the fuel meat swelling $\left(\frac{\Delta V}{V_0}\right)_{meat}$ can be expressed in Eqn. (4.13)

$$\left(\frac{\Delta V}{V_0}\right)_{meat} = \frac{V_{meat} - V_{meat}^{0}}{V_{meat}^{0}} = \frac{(V_{fuel} + V_{Al}) \times \left(1 - \left(\frac{\Delta V}{V_0}\right)_{porosity}\right) \times p_{fuel}^{0}}{V_{fuel}^{0}} - 1 \tag{4.13}$$

where p_{fuel}^{0} is the initial fuel loading fraction which is known from the fuel fabrication process.

Section 5

Thermal Model in DART-THERMAL

Thermal calculations are the backbone of fuel performance modeling since many phenomena affecting the fuel behavior under irradiation are related to the fuel temperature [19]. Therefore, a fuel performance model (fuel-matrix interaction, fuel swelling, etc.) has to be coupled with fuel temperature calculations to provide adequate predictions.

The thermal model within DART-THERMAL is a steady-state one-dimensional heat transfer model [5]. It assumes steady-state reactor operating conditions at each time step and a cosine power distribution along the axial direction. Thermal hydraulic conditions, power history and fuel geometry are defined for the thermal calculation. Several geometrical assumptions were made to facilitate the calculation: the thickness of the fuel meat and cladding are uniform; plate surface is flat; and the fuel plate has a perfect rectangular shape which ensures that symmetric boundary conditions can be applied. The temperatures at various interfaces (the water-oxide interface, the oxide layer-cladding interface, and the cladding-meat interface) as well as in the fuel meat are tracked through the calculation. The fuel meat is discretized into 8 zones in the thickness direction in the model. Since the plate is symmetric over the centerline, only the temperatures in half-meat-volume (5 zones) need to be calculated. The flow chart of the fuel temperature calculation subroutine is shown in Figure 5.1.

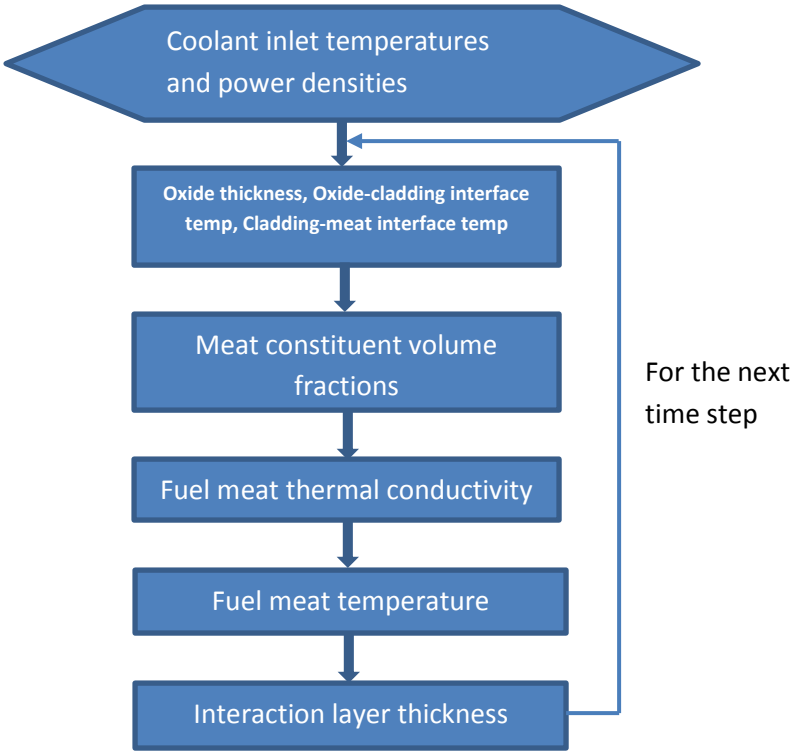

Figure 5.1 Flow chart of the fuel temperature calculation subroutine

5.1 Coolant temperature calculation

Coolant inlet temperature T_i and power density P (W/cm^3) at each time step (normally a full irradiation day) are specified in the input. The heat generated within a control volume is equal to the dissipated heat from that volume [5].

$$dq_{generated} = q_m \cdot \cos(\frac{\pi \cdot z}{2L_0}) \cdot dz = \rho(T) \cdot C_p(T) \cdot V \cdot Ac \cdot dT = dq_{dissipated} \quad (5.1)$$

where z the elevation position of the control volume in cm, L_0 the extrapolated length in cm, V the coolant velocity in cm/s, Ac the coolant channel cross section area in cm^2, and q_m the maximum linear power in W/cm which is calculated from the power density. The dependence of coolant density $\rho(T)$ (g/cm^3) and specific heat $C_p(T)$ (J/g-K) on temperature T was modeled using the following expression [20]:

$$\rho(T) \cdot C_p(T) \approx Amix \cdot \cos(\frac{\pi}{wmix}(T - T_c)) \quad (5.2)$$

where $Amix$, $wmix$ and T_c are fitting constants.

Use the fitting correlation in Eqn. (5.2) to replace the term of $\rho(T) \cdot C_p(T)$ in Eqn. (5.1), and do integration on both sides of Eqn. (5.1). The resultant expression is shown in Eqn. (5.3).

$$\int_0^z q_m \cdot \cos(\frac{\pi \cdot z}{2L_0}) \cdot dz = \int_{T_i}^{T_m(z)} Amix \cdot \cos(\frac{\pi}{wmix}(T - T_c)) \cdot V \cdot Ac \cdot dT \quad (5.3)$$

The coolant temperature $T_m(z)$ is therefore solved from Eqn. (5.3), and its expression is presented in Eqn. (5.4). $T_m(z)$ is stated as a function of axial distance z, the coolant inlet temperature T_i, and the linear power q_m.

$$T_m(z) = T_c + wmix/\pi \cdot \arcsin\left\{\frac{q_m \cdot 2L_0}{V \cdot Ac \cdot Amix \cdot wmix}\left[\sin\left(\frac{\pi \cdot z}{2L_0}\right) + 1\right] + \sin\left[\frac{\pi}{wmix}(T_i - T_c)\right]\right\} \quad (5.4)$$

where

- z : Elevation position of the control volume (cm)
- q_m : Maximum linear power (W/cm)
- L_0 : Extrapolated length (cm)
- V : Coolant velocity (cm/s)
- Ac : Coolant channel cross section area (cm^2)
- T_i : Coolant inlet temperature (K)

The formulation described above is a general expression and is suitable for many cases as long as T_i is provided.

In the current thermal model, only one node is utilized along the axial direction, which is too coarse to provide temperatures as a function of axial position. Hence, for the full-sized plate simulation, the code provides an average axial temperature. In order to obtain temperatures for any given axial position, it is necessary to specify the coolant inlet temperature of the simulated zone.

5.2 Oxidation layer surface temperature

The heat transfer coefficient between the bulk of the coolant and the oxidation layer surface is determined using the Dittus-Boelter correlation (shown in Eqn. (5.5)).

$$h(T) = 0.0243 \frac{V^{0.8}}{Dh^{0.2}} [\rho^{0.8} C_p{}^{0.4} k^{0.6} \mu^{0.4}] \tag{5.5}$$

where

$h(T)$: Heat transfer coefficient (W/(cm^2·K))

Dh : Hydraulic diameter (cm)

k : Coolant thermal conductivity (W/(cm·K))

μ : Coolant dynamic viscosity (Pa/s)

k, μ, ρ, and C_p in Eqn. (5.5) are all temperature dependent. In order to describe $h(T)$ as an explicit function of $T_m(z)$, a fitting correlation is introduced to simplify Eqn. (5.5):

$$h(T) \approx \frac{V^{0.8}}{Dh^{0.2}} Ah \cdot \sin[\frac{\pi}{wh}(T_m(z) - xch)] \tag{5.6}$$

here wh and xch are fitting constants.

The oxide layer surface temperature $T_{ox}(z)$ is given by the use of one-dimensional Fourier Law:

$$T_{ox}(z) = T_m(z) + q''(z) / h(T_m(z)) \tag{5.7}$$

where $q''(z)$ (W/cm^2) is the heat flux at the fuel plate surface. This heat flux is obtained from the power density P (W/cm^3) by:

$$q''(z) = P \times \frac{Vol_{meat}}{A_{meat}} \tag{5.8}$$

where Vol_{meat} (cm^3) and A_{meat} (cm^2) are the volume and the surface area of the fuel meat region, respectively. Plug Eqns. (5.6) and (5.8) into Eqn. (5.7), then $T_{ox}(z)$ can be written as:

$$T_{ox}(z) = T_m(z) + \frac{P \cdot Dh^{0.2} \cdot Vol_{meat}}{A_{meat} \cdot Ah \cdot V^{0.8} \cdot \sin[\frac{\pi}{wh}(T_m(z) - xch)]} \tag{5.9}$$

5.3 Oxidation layer-cladding interface temperature

The exposition of the cladding to both thermal and chemical coolant action enhances the growth of an oxide layer on its surface. Different parameters affect the growth of this oxide layer, namely coolant velocity, heat flux, surface temperature, coolant pH, and the presences of solutes. Several experimental correlations can be used to calculate the oxide layer thickness. DART-THERMAL allows the user to select an oxide growth correlation among Yeon Soo Kim's [21], Griess' [22] and Kritz's correlations.

Cladding temperatures are given by the use of one-dimensional Fourier Law,

$$T_{ox-Al} = T_{ox} + \frac{q''(z) \cdot ox}{k_{OX}} \tag{5.10}$$

where:

T_{ox-Al} : oxidation layer-cladding interface temperature (K)

T_{ox} : oxidation layer external surface temperature (K)

ox : oxidation layer thickness (cm)

$q''(z)$: heat flux across plate/rod thickness (W/cm^2) (shown in Eqn. (5.8))

k_{ox} : oxidation layer thermal conductivity (mostly considered to be boehmite) (W/(cm·K))

5.4 Cladding-fuel meat interface temperature

The cladding-fuel meat interface temperature is calculated in the same fashion as T_{ox-Al} . The equation for $T_{Al-fuel}$ is expressed as:

$$T_{Al-fuel} = T_{ox-Al} + \frac{q''(z) \cdot CL}{k_{cladding}} \tag{5.11}$$

where

$T_{Al-fuel}$: cladding-fuel meat interface temperature (K)

CL : cladding thickness (cm)

$k_{cladding}$: cladding thermal conductivity (W/(cm·K))

$q''(z)$: heat flux across plate/rod thickness (W/cm^2) (shown in Eqn. (5.8))

5.5 Fuel meat temperature

In order to perform an accurate thermal calculation for the fuel meat, the fuel meat region is discretized into 8 zones along the thickness direction. Materials properties (thermal conductivities) and important attributes (constituent volume fractions, fuel particle morphology, and fuel-matrix interaction thickness) are tracked as the increase of irradiation time. Fuel meat temperature of each zone is calculated as:

$$T_{meat(n)} = T_{meat(n-1)} + \frac{q''(z) \cdot Th_{meat} / 8}{k_{meat(n)}} \qquad \text{(n=2,...,5)} \qquad (5.12)$$

where $T_{meat(1)} = T_{Al-fuel}$; $T_{meat(5)}$ is the centerline temperature. Th_{meat} is the meat thickness in cm, and $k_{meat(n)}$ is the thermal conductivity of the nth zone.

Figure 5.2 shows a representative example of calculated temperatures across the fuel plate with DART-THERMAL. Time evolution of temperatures at various fuel locations are depicted for V6018G fuel plate from the RERTR-5 experiment.

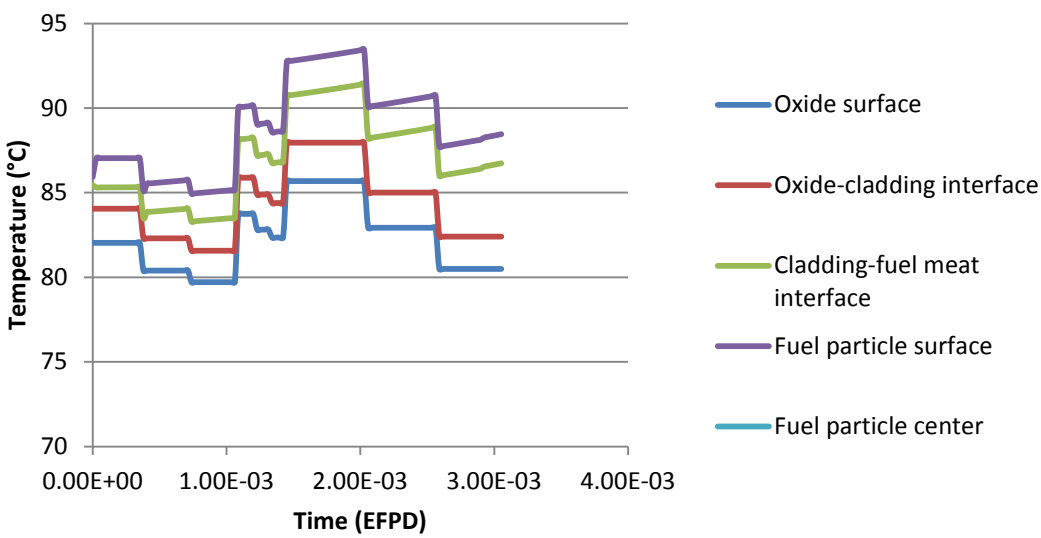

Figure 5.2 Temperatures across the RERTR-5 V6018G fuel plate calculated with DART-THERMAL

Section 6

Model Validation Against RERTR-5 Experimental Data

6.1 Operational conditions and fuel fabrication parameters

Three fuel plates from RERTR-5 test were selected for DART-THERMAL validation study. The selected plates were the only ones among RERTR-5 fuel plates that were fabricated with atomized U10Mo powder and have available PIE data. Their dimension is 100 mm x 25 mm x 1.4 mm. The fuel plates were irradiated in the ATR for 116 EFPD with a peak U-235 burnup of 52%. Table 6.1 summarizes fuel design parameters and operational conditions for the RERTR-5 test, and Table 6.2 lists the specific fabrication and irradiation information for the selected fuel plates.

Table 6.1 Design parameters and operational conditions for the mini fuel plates in RERTR-5 test [23]

Fabrication parameters	
Fuel type	UMo/Al dispersion fuel
U-235 enrichment (at%)	19.5
U-loading (gU/cm^3 meat)	6 - 8
Fuel particle shape	spherical
Fuel Geometry	plate
Plate length (mm)	100
Plate thickness (mm)	1.40
Plate width (mm)	25
Meat thickness (mm)	0.635
Meat length (mm)	81.28
Cladding thickness (mm)	0.381

Operation conditions	
Coolant velocity (m/s)	6
Coolant PH (BOL)	~5.3
Coolant channel width (mm)	23.12
Coolant channel thickness (mm)	1.232
Coolant inlet temperature (°C)	52 - 73
Cycle length (EFPD)	116
Peak Burnup (at% LEU U-235)	52

Table 6.2 Fabrication and irradiation information of the selected RERTR-5 fuel plates [23]

Plate ID	AGHCF number	U-loading (gU/cm^3 meat)	Measured burnup (%^{235}U)	Fission density (10^{21} f/cm^3)	Inlet coolant temperature (°C)
V6018G	600D	6	35.78	2.30	52
V6019G	600M	6	45.47	2.95	57
V8005H	600AH	8	37.0	2.38	73

Fuel particles have a size distribution resulting from the fabrication process. Since the atomized powder was from the same manufacturing batch, the same initial fuel particle size distribution (as shown in Table 6.3) was applied for all fuel plates from the RERTR-5 test.

Table 6.3 Fuel particle size distribution

Fuel particle diameter (μm)	Distribution frequency (%)
128.0	6.0
90.5	24.6
69.0	20.0
54.0	27.2
41.5	9.6
30.0	12.6

Post irradiation examination (PIE) was carefully performed after the fuel plates were taken out from the reactor. Fuel thickness increase, constituent volume fractions, and interaction layer (IL) thickness were measured. Table 6.4 describes measurement data for the three fuel plates, which are used in this validation study.

Table 6.4 Measured volume fractions and total meat swelling for the select RERTR-5 fuel plates

Plate ID	As-fabricated fuel vol.%	Postirradiation measurement				
		Fuel vol.%	Reaction product vol.%	Aluminum vol.%	IL thickness (μm)	Average meat swelling (%)
V6018G	39.2	38.2	33.9	28	7.5	9
V6019G	39.2	34.5	50.8	15	13.5	15
V8005H	51.9	47.4	43.2	10	11.5	12

6.2 Results and discussion

The constituent volume calculation in DART-THERMAL is conducted on the basis of interaction layer growth which is a function of the temperature and fission rate. A recently improved correlation, based on RERTR-4 and RERTR-5 PIE measurements [24], has been incorporated into DART-THERMAL. This correlation has a form of

$$\Delta y^2 = 5.0\times10^{-17}\exp(-7000/RT)\,\dot{f}^{1/2}\Delta t \qquad (6.1)$$

where Δy is the interaction layer growth (cm); R = 1.987 cal/mol·K is the gas constant; T is the fuel temperature in K; $\dot{f}$ is the fission rate (fission/s-cm^3); and Δt is irradiation time (s) [24].

Figure 6.1 shows the comparison between calculated and measured interaction layer thicknesses for three RERTR-5 fuel plates. Calculated IL thicknesses for V6018G and V6019G are consistent with the measurement (listed in Table 6.4), and the calculated value for V8005H interaction layer thickness is within its measurement error range.

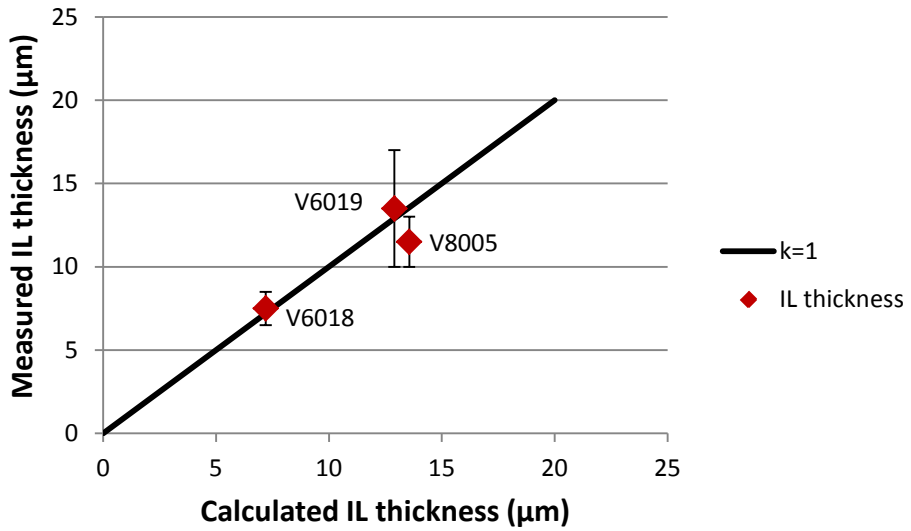

Figure 6.1 Comparison of calculated and measured interaction layer thicknesses for the selected RERTR-5 fuel plates

Figure 6.2 shows a comparison of calculated and measured constituent volume fractions and fuel meat swelling for the selected RERTR-5 fuel plates. The corresponding calculation results are listed in Table 6.5. Figure 6.2 and Table 6.5 indicate reasonable consistency between calculated and measured total meat swelling and fuel volume fraction. The DART-THERMAL model slightly over-predicted the Al volume fractions for V6018G and V6019G, and under-predicted this quantity for V8005H.

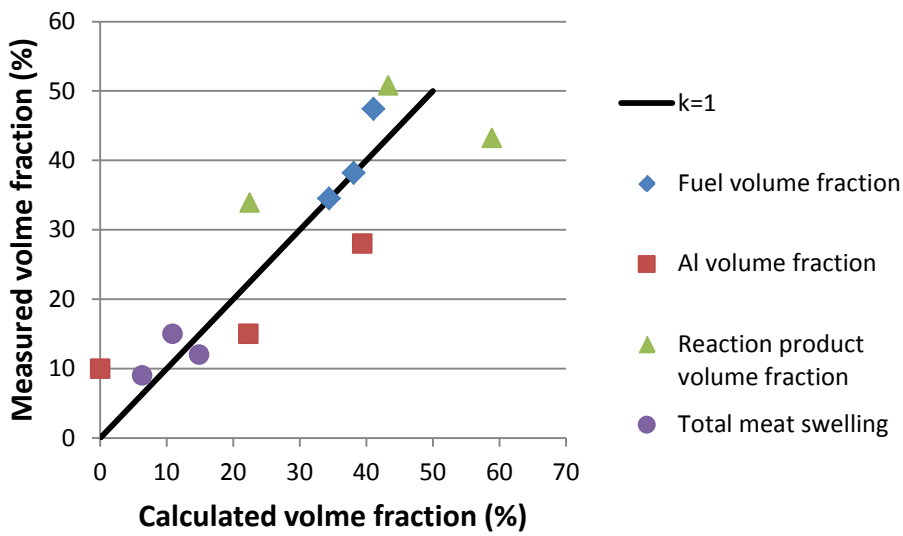

Figure 6.2 Comparison of calculated and measured constituent volume fraction and total meat swelling for the selected RERTR-5 fuel plates

Table 6.5 DART-THERMAL calculated constituent volume fraction, total meat swelling and IL thickness for the selected RERTR-5 fuel plates

Plate ID	Fuel vol.%	Reaction product vol.%	Aluminum vol.%	IL thickness (μm)	Average meat swelling (%)
V6018G	38.1	22.5	39.4	7.2	6.3
V6019G	34.4	43.3	22.3	12.9	10.9
V8005H	41.1	58.9	0	13.6	14.9

Compared to V6018G and V6019G, V8005H has a much higher initial fuel volume fraction due to its higher uranium loading, which leads to a higher interaction rate between fuel and matrix. By the end of the calculation, most of the matrix Al was consumed for plate V8005H. This was confirmed by PIE inspection. Figure 6.3 is a micrograph of plate V8005 after irradiation. It shows that in most regions, the Al matrix was consumed and replaced with interaction layer. Large pores are also clearly shown in many regions of the fuel matrix. These fission-gas-filled pores are normally located between the interaction layer and the Al matrix. These large pores thus tend to isolate the remaining matrix Al from the fuel particles and, as such, provide barriers to subsequent interaction between the fuel particle and the Al matrix. A portion of the Al matrix is therefore conserved. In the current version of DART-THERMAL, there is no physical model to describe the blocking action of these large fission-gas-filled-pores, which is a possible contribution to the resultant small discrepancy.

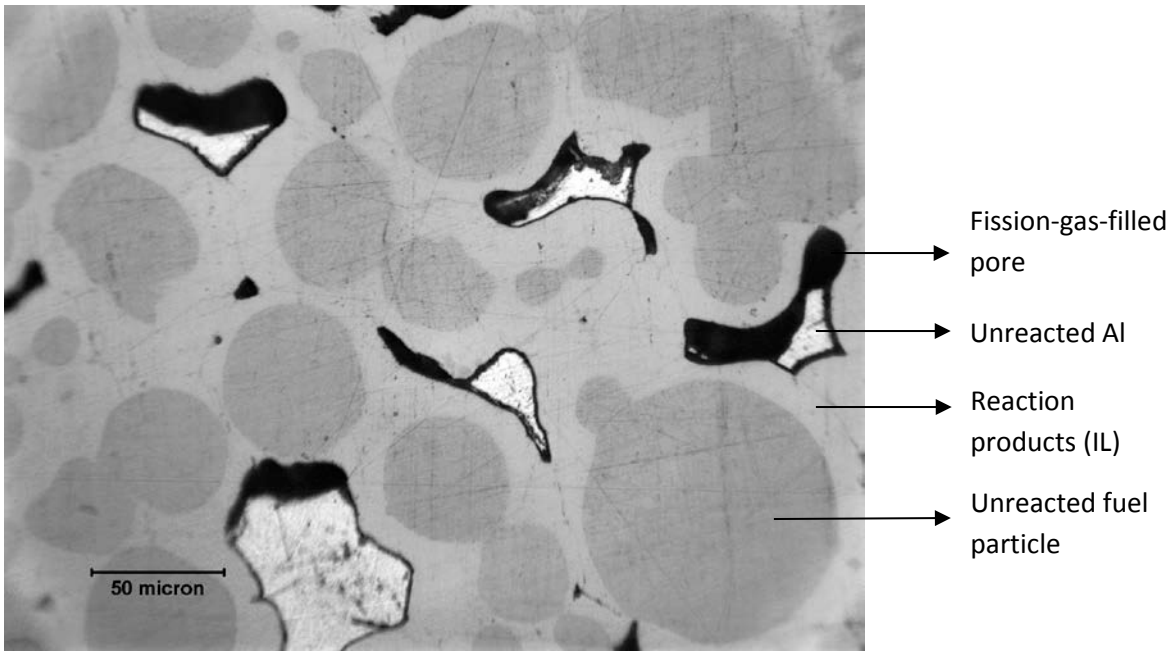

Figure 6.3 Micrograph taken on RERTR-5 V8005H miniplate showing the Al in matrix was converted to reaction products.

Section 7

Validation Against RERTR-6, 7, 9 Test Data

7.1 Operational conditions and fuel fabrication parameters

RERTR-6, 7 and 9 tests were conducted in the ATR at the INL. The fuel plates used in these tests have the same geometry dimensions and configurations as the plates used in RERTR-5. Therefore, the same thermal-hydraulic conditions, core configurations and fuel geometries are used for simulating RERTR-5, 6, 7, and 9 tests. Irradiation data for RERTR-5, 6, 7, and 9 fuel plates chosen for the current analysis are listed in Table 7.1.

Table 7.1 RERTR-5, 6, 7 and 9 test data [17]

Test	Plate ID	Fuel/matrix composition	Nominal U loading (gU/cm^3)	U-235 enrichment (%)	Time (EFPD)	Avg fuel particle diameter (µm)	Life avg T (°C)	Life avg FR (10^{14} f/cm^3-s)	Measured IL thickness growth (µm)
RERTR-5	V6018G	U-10Mo/Al	6	19.5	116	65	80	2.29	7.5
	V6019G	U-10Mo/Al	6	19.5	116	65	96	2.91	13.5
	V8005G	U-10Mo/Al	8	19.5	116	65	109	2.37	11.5
RERTR-6	R5R020	U-7Mo/Al-0.2Si	6	19.1	135	65	105	2.67	9.5
	R1R010	U-7Mo/Al-1Si	6	19.5	135	65	87	2.34	2.0
	R2R020	U-7Mo/Al-2Si	6	19.4	135	65	93	2.64	1.9
	R3R030	U-7Mo/Al-5Si	6	19.1	135	65	95	2.57	1.5
RERTR-7	R2R050	U-7Mo/Al-2Si	6	58.2	90	90	134	5.12	9.5
	R3R040	U-7Mo/Al-5Si	6	58.3	90	80	117	5.70	2.0
RERTR-9	R2R088	U-7Mo/Al-2Si	8.5	58.1	115	50	153	5.64	8.5
	R6R018	U-7Mo/Al-3.5Si	8.5	58.1	115	50	154	5.49	6.5

Starting from the RERTR-6 test, Si was added into the Al matrix in order to reduce the development of the fuel-matrix interaction layer. The interaction layer growth correlation described in Eqns. (4.1-4.4) was applied in the validations against these RERTR test data. The correlation takes into account the Si addition effect. In order to access the fuel performance at extreme irradiation conditions, the RERTR-9 test used fuel particles with high U-235 enrichment and high U loading. Thus, these fuel plates reached very high fuel temperatures (> 150°C) and high burnup during their life time. Fuel particles in RERTR-7 and 9 fuel plates have different size distributions from the particles used in RERTR-5 and 6 tests, since they were fabricated by different manufacturers.

7.2 Results and discussion

Comparisons of calculated and measured IL thickness, fuel meat swelling, and constituent volume fractions for RERTR tested fuels are shown in Figure 7.1, 7.2, and 7.3 respectively. The results presented

in Figure 7.1-7.3 consist of data obtained from RERTR-5, 6, 7 and 9 tests. The results are organized into two categories for clarity: fuel plates with pure Al matrix, and fuel plates with addition of Si in the Al matrix. The calculated data presented in the following three figures were obtained with DART-THERMAL.

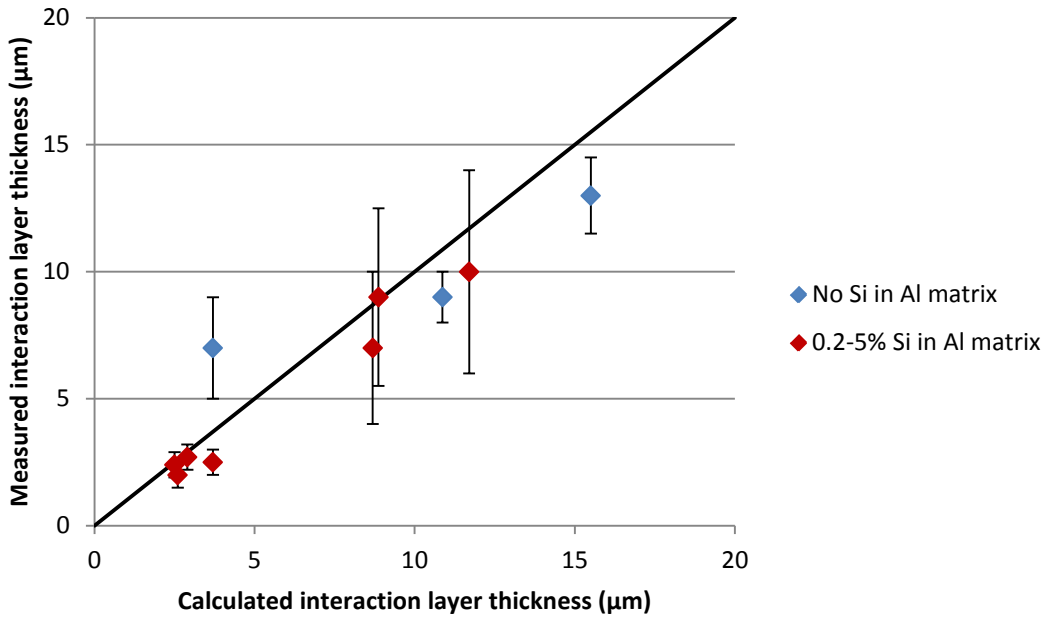

Figure 7.1 Comparison of the calculated and measured interaction layer thickness for the selected RERTR tested fuels

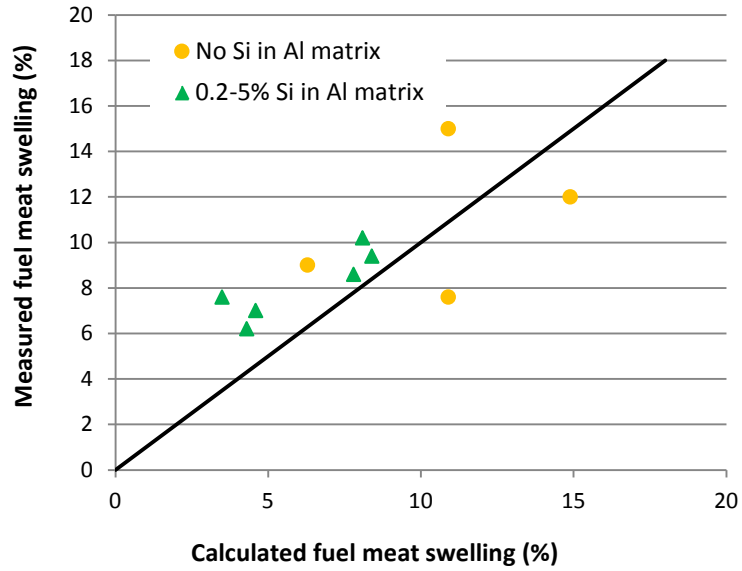

Figure 7.2 Comparison of the calculated and measured fuel meat swelling for the selected RERTR tested fuels

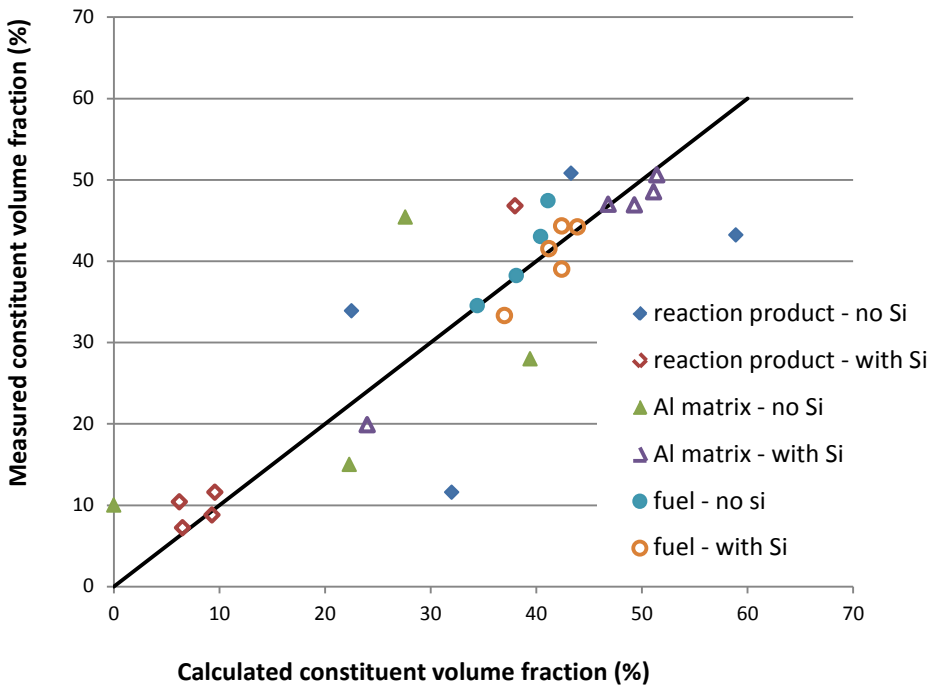

Figure 7.3 Comparison of the calculated and measured fuel meat constituent volume fractions for the selected RERTR tested fuels

The measurement errors indicated in Figure 7.1 reflect the irregularity of IL thickness. The errors tend to be larger for the samples with a Si-added matrix than for the pure Al matrix samples. Characterization of

as-fabricated plates showed that IL growth occurred during fabrication processes for RERTR fuels. This is because the hot rolling technique used to fabricate RERTR fuel plates involves heating steps at ~500°C for a total of an hour. The estimated IL growth during fabrication is 1.5 µm for plates with pure Al matrix and 0.5 µm for plates with Si-addition in the Al matrix. The data shown in Figure 7.1 include the as-fabricated IL thicknesses.

The measured fuel swelling data is obtained by measuring the change of fuel plate thickness before and after irradiation. As shown in Figure 7.2, the model slightly underpredicts the fuel meat swelling in the fuel plates with Si addition in the matrix. This discrepancy might be related to uncertainties associated with the fuel swelling contribution from pores located between fuel particles and ILs. The current model for these interfacial fission-gas-filled pores will be improved and updated in the next version of DART-THERMAL.

The calculated reaction product volume fractions shown in Figure 7.3 do not include the as-fabricated IL formation. The change in calculated reaction product volume fraction when the as-fabricated IL is included is around 0.2%, which is negligible comparing to the total reaction product volume fraction.

Reasonable agreement between calculation and measurement is demonstrated for interaction layer thickness, fuel meat swelling, and fuel meat constituent volume fractions. These results demonstrate that the model of IL formation and the temperature subroutine are correctly implemented in DART-THERMAL, and that the model is able to predict the RERTR test results with reasonable accuracy.

Section 8

AFIP-1 Full-Sized Plate Test

8.1 Experiment description

The Advanced Test Reactor Full size plate In center flux trap Position (AFIP) experiment AFIP-1 was designed to demonstrate the performance of U-Mo dispersion fuels at a full-size scale with a length of 21.5 (54.6 cm) inches, width of 2.25 (5.75 cm) inches and a thickness of 0.050 (0.13 cm) inch for each fuel plate. In the AFIP-1 experiment, two full-size fuel plates (1T2 and 1B5) were irradiated, with one stacked above the other and welded into an aluminum frame (Figure 8.1). The experiment matrix for AFIP-1 is listed in Table 8.1.

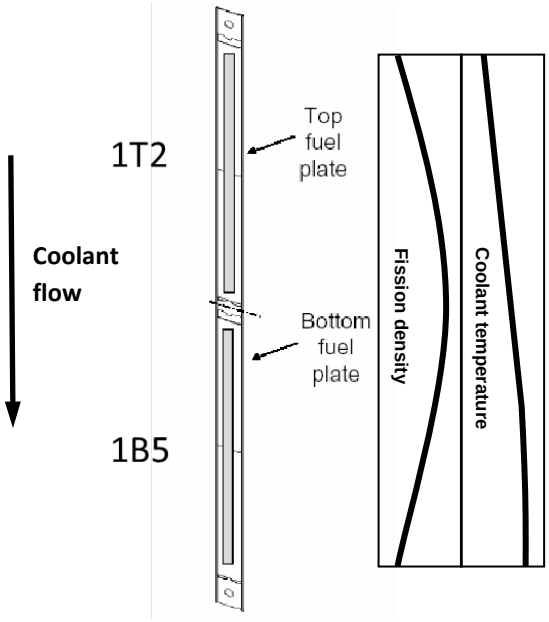

Figure 8.1 AFIP-1 plate loading configuration with schematic distribution profiles of the fission density and coolant temperature

Table 8.1 Experiment matrix for AFIP-1

Fuel Plate ID	1T2	1B5
Fuel Plate Location	Top	Bottom
Fuel Type	U-7Mo Dispersion	U-7Mo Dispersion
Fabrication Method	Roll Bonded	Roll Bonded
Matrix Materials	Al-2Si	Al-4043 (5Si)
Uranium Loading (g/cc)	8	8
Uranium-235 Enrichment (%)	19.5	19.5

Table 8.2 lists the nominal fuel plate dimensions and thermal-hydraulic conditions. The fuel plates in AFIP-1 test were irradiated for a total of 158.2 EFPD, consisting of three irradiation cycles: 142A, 143A and 143B.

Table 8.2 Experimental parameters: fuel dimensions and operational conditions [25]

Fuel Dimensions	
Plate Length (mm)	546.1
Plate Width (mm)	57.15
Plate Thickness (mm)	1.27
Meat Length (mm)	523.88
Meat Width (mm)	36.83
Meat Thickness (mm)	0.56
Cladding Thickness (µm)	354.33
Thermal-hydraulic Conditions	
Coolant velocity (m/s)	10.36
Coolant PH (BOL)	~5
Coolant channel width (mm)	48.4
Coolant channel thickness (mm)	5.08
Coolant inlet temperature (°C)	52
Irradiation Cycles	
142B (EFPD)	52.0
143A (EFPD)	48.9
143B (EFPD)	57.3

The fuel particles were supplied by KAERI and were fabricated by using the same manufacturing procedure as that used for the RERTR-5 test. Therefore the same fuel particle size distribution used for RERTR-5 was assumed.

After irradiation, two strips of meat material were sectioned from each fuel plate at various elevation positions as indicated in Figure 8.2. Post irradiation examinations (PIE) were carried out on each of these strips to reveal detailed microstructural changes after irradiation. Multiple areas were selected for optical microscopy (OM) and scanning electron microscopy (SEM) observation. Constituent volume fractions were measured based on SEM micrographs, which are compared with simulation results in this study, as well as with fuel meat swelling data.

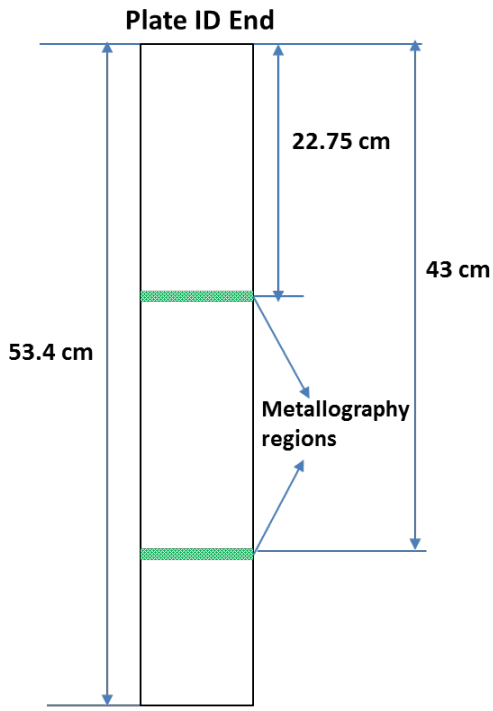

Figure 8.2 AFIP-1 section diagram for PIE

8.2 Power history and coolant temperature

As-run neutron and thermal analysis data calculated by Idaho National Laboratory [25] were used in the DART-THERMAL calculation. Power history at each specific PIE region was described by the evolution of fission density in the fuel particles during the irradiation test (shown in Figure. 8.3). The fission density in the fuel particles was derived based on MCNP-calculated U-235 burnup presented in [25].

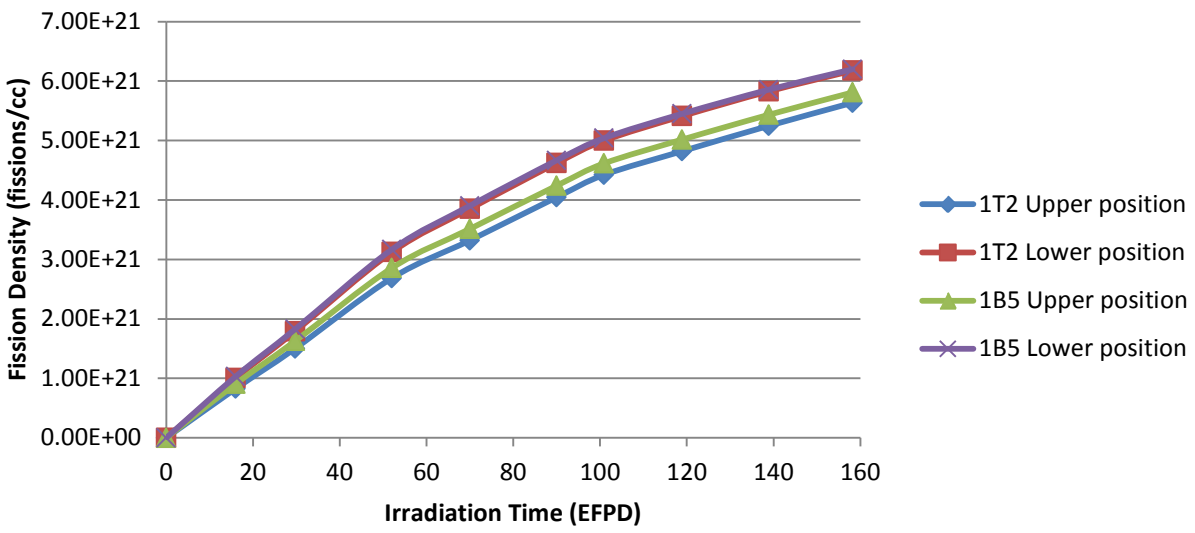

Figure 8.3 Evolution of fission density in fuel particles during the irradiation experiment at various PIE positions

Coolant channel temperatures were calculated with ABAQUS [25]. There were three coolant flow channels in the test assembly, designated as the left, the center, and the right coolant channel respectively. The AFIP-1 fuel plates were located between the left and the center coolant channels. In order to provide a conservative estimate of the test results, the higher coolant channel temperature at each irradiation time step was consistently chosen for the simulations. The coolant temperatures for each specific PIE position during irradiation cycles are listed in Table 8.3.

Table 8.3 Coolant temperatures at various PIE positions

Operation cycle	Irradiation time (EFPD)	Coolant temperature (°C)			
		1T2 upper	1T2 lower	1B5 upper	1B5 lower
142B	0	54.0	58.0	53.2	55.6
	16	54.4	58.0	53.2	55.6
	29.7	54.4	58.4	53.4	56.0
	52	54.4	57.6	53.4	55.6
143A	52	52.8	54.8	52.8	54.8
	70	53.0	55.0	53.0	55.0
	90	53.2	55.0	53.2	55.0
	100.9	53.0	54.8	53.0	54.8
143B	100.9	54.0	57.6	52.6	54.0
	118.9	54.2	58.0	52.7	54.0
	138.9	54.4	57.6	52.6	54.0
	158.9	54.0	57.0	52.6	54.0

8.3 Results and discussion

Results of the DART-THERMAL code calculation compared with measured data for both fuel plates from the AFIP-1 test are shown in Figures 8.4 and 8.5. The comparison shows that the calculated fuel meat constituent volume fractions and swelling are in a good agreement with the measured values. These results indicate that DART-THERMAL is capable of capturing the overall fuel microstructural evolution under AFIP-1 experimental conditions. Together with the validation results of RERTR mini-plate tests in the previous sections, the validation results demonstrate that the DART-THERMAL code can simulate fuel microstructural evolution not only in mini-size fuel plates at lower fission rates and irradiation temperatures, but also in full-sized fuel plates under more extreme irradiation conditions.

Relatively large pores in the Al matrix due to fabrication were observed in the AFIP-1 fresh fuel plates. These pores barely changed during irradiation. Around 2 vol% of fuel meat remained as fabrication voids. On the contrary, a phenomenon called irradiation-enhanced sintering is often observed in uranium silicide fuels and U-Mo mini-plates: the as-fabricated pores disappear after irradiation due to fuel particle swelling. The different behavior of as-fabricated pores between AFIP-1 fuel plates and other fuel plates might result from their different locations in the fuel meat. In uranium silicide fuels or U-Mo mini-plates, as-fabricated pores exist normally either in fuel particles or at the interfaces of fuel particles and Al matrix. In contrast, the pores stay within the matrix in AFIP-1 fuels due to the slightly different manufacturing processes. However, the remaining large pores in AFIP-1 fuels are not reflected in the current model which was developed based on uranium silicide fuels. In order to account for this effect in the DART-THERMAL calculations, the fuel meat thermal conductivity, some porosity (2 vol% of meat) was artificially added back into the meat. This correction can cause slight change in the calculated fuel temperature by 1-2°C, and eventually alter the meat constituent volume fractions by 1-2 vol%.

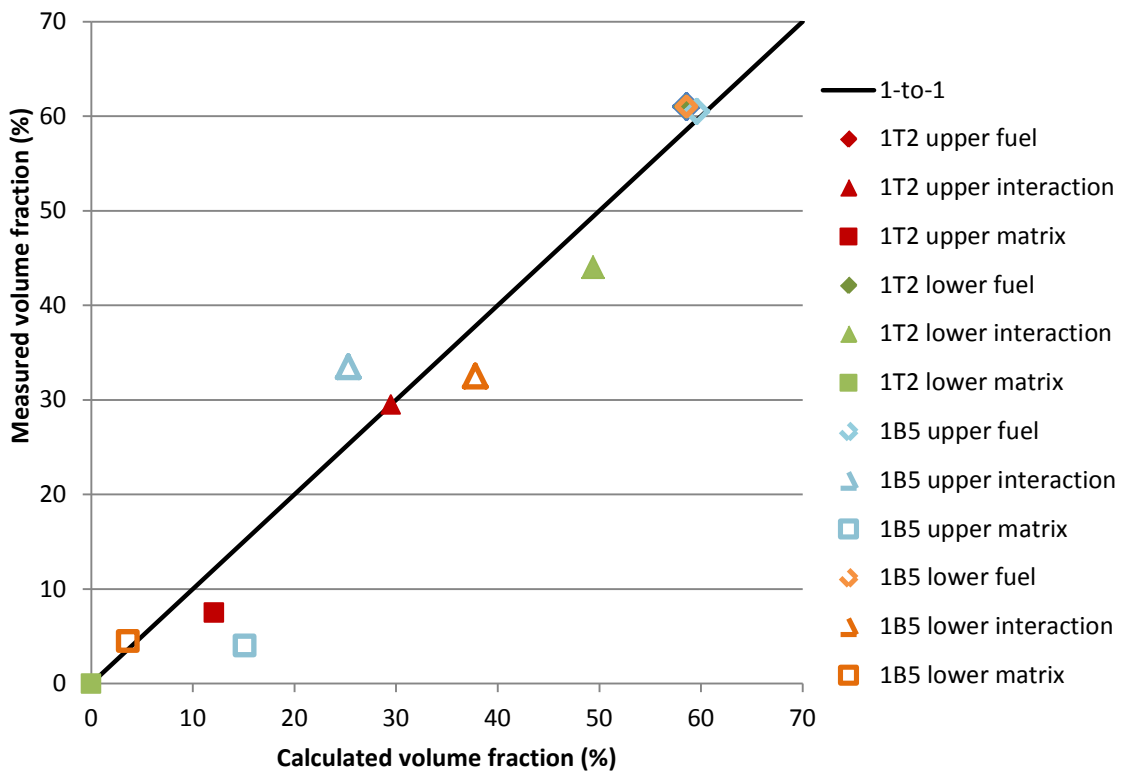

Figure 8.4 Comparison of calculated and measured constituent volume fractions for AFIP-1 test.

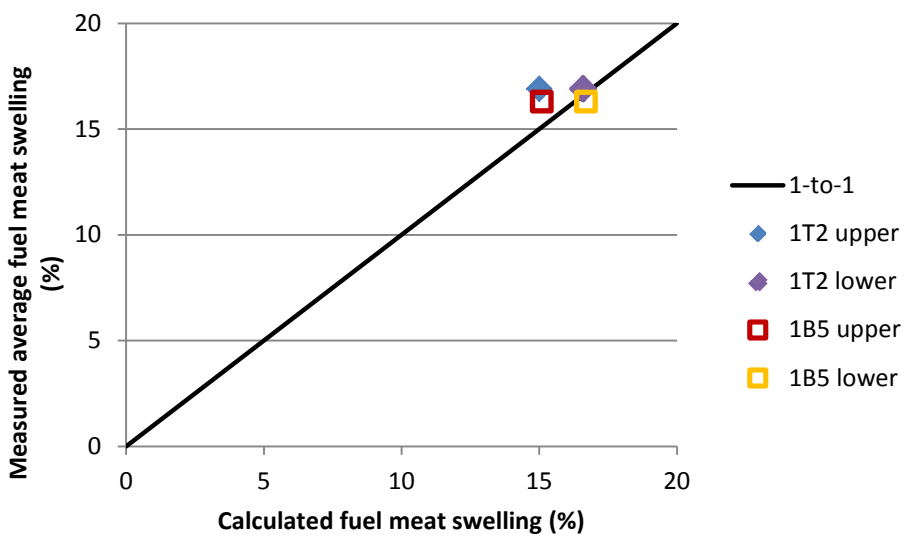

Figure 8.5 Comparison of calculated and measured fuel meat swelling for AFIP-1 test.

There is a relatively large discrepancy between calculated and measured data that takes place at the 1B5 upper location (Figure 8.4). The calculation resulted in 15.1 vol% of fuel meat that remained as unreacted Al matrix, while there was only 4 vol% from the measurement. This difference suggests that the code underestimates Al consumption for this location. Correspondingly, the interaction product

volume fraction was also underestimated. The fuel volume fraction agreed with the measurement. Careful investigation was performed for the purpose of understanding this discrepancy. Several reasons were determined to be potentially responsible for the underestimation of Al matrix: inaccurate measurement of interaction product composition, oxidation layer thickness, or coolant temperature at the PIE position. The detailed analyses are described as follow:

(1) Interaction product composition

The composition of reaction product formed between U-Mo alloy and Al-Si matrix has a form of $(U_aMo_{1-a})(Al_bSi_{1-b})_x$, where x ranges from 3 to 7. Since the formation of an interaction layers is the result of fission-induced interdiffusion, the composition of the reaction product evolves during irradiation. There is no measured data for the density of the reaction product. The densities used in DART-THERMAL were estimated from UAl_x [26]. In order to examine the influence of interaction product composition, two potential compositions were compared for AFIP-1 test at 1B5 upper location: $(U_{0.8}Mo_{0.2})(Al_{0.6}Si_{0.4})_{3.7}$ and $(U_{0.8}Mo_{0.2})(Al_{0.6}Si_{0.4})_7$. Their estimated densities are 6.3 g/cm^3 and 4.52 g/cm^3 respectively. Surprisingly, these two compositions give almost identical results. The reason for this is that the formation of $(U_{0.8}Mo_{0.2})(Al_{0.6}Si_{0.4})_{3.7}$ takes place earlier in the calculation than $(U_{0.8}Mo_{0.2})(Al_{0.6}Si_{0.4})_7$ due to less matrix material required for formation. As the fuel converts into interaction product, the thermal conductivity of the converted region decreases significantly. Such decrease in the thermal conductivity results in an increase in fuel temperature. The increased fuel temperature then accelerates interaction layer growth. Hence, the $(U_{0.8}Mo_{0.2})(Al_{0.6}Si_{0.4})_{3.7}$ interaction product has a higher calculated growth rate than $(U_{0.8}Mo_{0.2})(Al_{0.6}Si_{0.4})_7$. It compensates the lower matrix consumption ratio as compared to $(U_{0.8}Mo_{0.2})(Al_{0.6}Si_{0.4})_7$.

(2) Oxidation layer thickness

An oxide film develops on the surface of Al cladding during reactor operation. This oxidation layer can pose a considerable performance issue for the dispersion fuel owing to its low thermal conductivity (~ 10-fold lower than that of Al). As determined from the previous RERTR test data, the oxide growth is a function of irradiation time, coolant temperature, fission rate, and pH value [27]. The growth of oxide layers was not substantial in the ATR as compared to other reactors with similar power, which is probably a result of the relatively low pH of the primary coolant water. The measured oxide thickness profile in the AFIP-1 test showed that the maximum value (< 10 μm) appeared near the center of the coolant channel, and the lowest values at both ends. Big variations (~5 μm) in oxidation layer thickness measurement were observed even at the same elevation along the coolant channel. This could be due to the uneven wavy nature of the oxide layer. A sensitivity study was therefore conducted in order to reveal any oxide thickness effect. Three various oxide thicknesses were used as input, and the calculated results are listed in Table 8.4.

Table 8.4 Sensitivity study results on the oxide thickness at the 1B5 upper location

		Calculated values			Measured data
Oxide thickness (µm)		5.08	10.08	12.7	2.8-6.4
Volume fractions (%)	Fuel	59.6	60.7	60.2	61.5
	Interaction product	25.3	28.2	30.5	33.5
	Matrix	15.1	11.2	9.3	4
	Porosity	0	0	0	2
Fuel meat swelling (%)		15.1	16.0	15.7	16.3

The results listed in Table 8.4 show that the Al matrix consumption increases when the oxide layer gets thicker. This trend results from the higher fuel temperature achieved with a thicker oxide layer. The code calculation shows the fuel temperature increases ~ 7°C when the oxide thickness rises from 5.08 µm to 12.7 µm. At an oxide thickness of 12.7 µm, the calculated constituent volume fractions are in close agreement with the measured data. Although it is not realistic to use such a large value for oxide thickness in the calculation, since the measured oxide thickness does not exceed 10 µm, this result is useful for understanding the discrepancy between measured and calculated data. It seems that the fuel temperatures might be somewhat underestimated in the calculation for the 1B5 upper location, but it is not a result solely caused by uncertainties in oxide thickness measurement.

(3) Coolant temperature

The coolant temperature has a direct impact on the fuel temperature. Inaccurate coolant temperature measurement can have a significant impact on the fuel temperature calculation. Unfortunately there is no measured coolant temperature available from the test. The information used in the DART-THERMAL analysis thus comes from the thermal analysis based on the MCNP-calculated surface heat flux, as-built geometry and nominal coolant channel flow rate as described in [25]. A re-examination of the thermal analysis was performed by comparing the thermal conditions between the AFIP-1 and RERTR-7 tests, since they share the same coolant flow rate. The plate R3R050 from RERTR-7 was located at a comparable position (C7) in the reactor as the 1B5 upper location. The coolant temperatures were estimates based on generated heat fluxes, coolant channel dimensions and coolant flow rate for these two cases. The results of this analysis demonstrate that the calculated coolant temperatures reported in [25] are reasonable.

As such, there is no single reason found to explain the slight underestimation of Al consumption for the 1B5 upper location. The main error source can be traced back to fuel temperature. Considering the very limited availability of data points (only 4) from this test, further investigation is required in order to make a more definitive conclusion on the discrepancy.

Section 9

Proposed Application of U_3Si_2/Al Dispersion Fuel in RHF

The Institut Laue-Langevin (ILL), Grenoble, France, is considering U_3Si_2 dispersion fuel as an alternative to U-Mo for the conversion of their High Flux Reactor (RHF). With some modifications to the fuel plate design, a fuel loading of 6 gU/cm^3 appears to be needed [28]. Because the testing and operating experience with U_3Si_2 at higher loading is very limited, it is necessary to access the irradiation performance of proposed U_3Si_2/Al fuel for RHF conditions by using simulation methods. This exercise will serve to demonstrate the versatility of DART-THERMAL for dispersion fuel performance analysis.

9.1 Parameters applied in the calculations for RHF fuel

The operation conditions of RHF and the proposed design parameters of U_3Si_2/Al dispersion fuel used in RHF are listed as below (Table 9.1).

Table 9.1 RHF operating conditions and design parameters for proposed application of U_3Si_2/Al dispersion fuel in RHF

Operating parameters	
Total power (MW)	57.81
Cycle length (days)	48
Burnup (at% LEU U-235)	51
Fission density (10^{21} f/cm^3)	2.6
Max fuel temperature, BOL (°C)	150
Max fuel temperature, EOL (°C)	120
Max heat flux, BOL (W/cm^2)	450
Max heat flux, EOL (W/cm^2)	150
Fuel fabrication	
Fuel type	U_3Si_2/Al dispersion fuel
U-235 enrichment (at%)	19.75
U-loading (gU/cm^3 meat)	6
Fuel Geometry	plate
Plate length (mm)	903
Plate thickness (mm)	1.27
Plate width (mm)	82
Meat thickness (mm)	0.61
Meat length (mm)	880
Clad thickness (mm)	0.33
Coolant properties	
Coolant	D_2O
Coolant velocity (m/s)	17
Inlet temperature (K)	311.15

Outlet temperature (k)	~325
Pressure inlet (bar)	~14
Pressure outlet (bar)	~4
Coolant PH (BOL)	~5.5
Coolant PH (EOL)	~5

9.2 Calculation results

An average fuel particle size of 70 micron was used in the calculations. The smaller fuel particle size is, the more Al reacts with fuel and results in thicker IL.

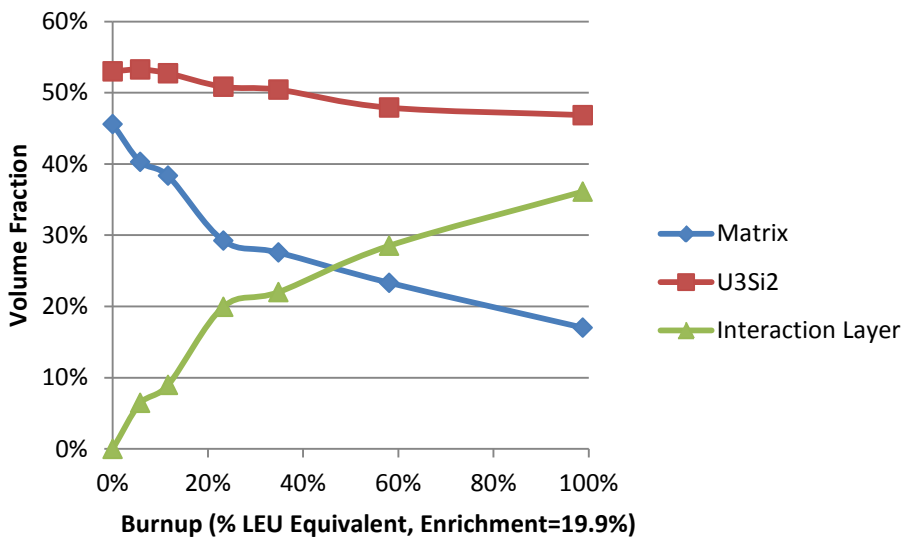

Figure 9.1 Evolution of constituent volume fractions in U_3Si_2/Al dispersion fuel with burnup

It is seen from Figure 9.1 that at the end of life, considerable Al matrix volume fraction (~18%) still remains. Judging from this prediction, the proposed design condition to use U_3Si_2 dispersion for RHF is acceptable from fuel performance point of view. The calculation result of growth of IL thickness of U_3Si_2 fuel particle during irradiation is shown in Figure 9.2.

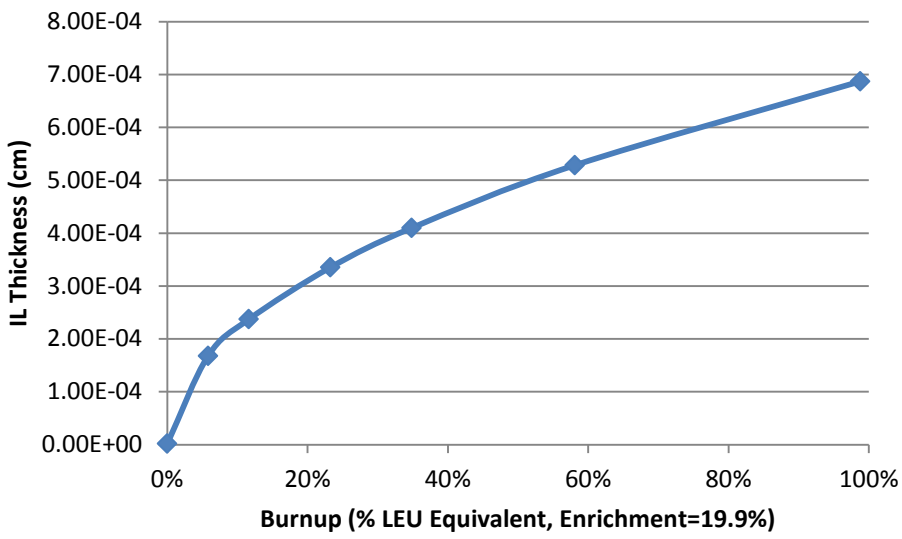

Figure 9.2 Growth of IL thickness of U_3Si_2 fuel particle with burnup

The results show that at 100% burnup ~17% of total meat volume of fuel is Al matrix, and IL thickness is 6.8 µm. Based on this estimation, the proposed application of U_3Si_2/Al dispersion fuel in RHF is acceptable.

Section 10

Summary and Future Work

The fuel performance code DART-THERMAL has been developed to simulate the irradiation performance of high-density U-Mo/Al dispersion fuel plates. Performance predictions are based on a mechanistic gas-driven-swelling model and some empirical correlations developed using extensive PIE data from the RERTR tests. DART-THERMAL calculates fuel meat temperatures as a function of changes in fuel meat thermal conductivity and oxide layer thickness during irradiation. A key feature of DART-THERMAL is its capability to calculate the fuel meat thermal conductivity as a function of changes in the fuel microstructure, morphology, and chemistry that is, in turn, dependent upon fission density, temperature and irradiation time.

Validation results for DART-THERMAL against PIE data obtained from RERTR tests -5, 6, 7, 9 and AFIP-1 show good overall agreement between calculated and measured data. As such, DART-THERMAL is a viable tool for U-Mo/Al dispersion fuel performance analyses.

Several limitations have been found in the current model. These limitations reduce the flexibility of DART-THERMAL for fuel performance analysis. Therefore, the future development of the DART-THERMAL code will be focused at improving its capability for modeling swelling phenomenon in MTR-type dispersion fuel. In the near term, code development will focus on two aspects.

The first aspect is interfacing DART-THERMAL with the thermal solution code PLTEMP. The current version of DART-THERMAL has two drawbacks associated with the temperature calculations. One of them is that the code lacks the capability to calculate the temperatures at specific positions in the fuel plate. Thus the coolant temperature at the simulated position has to be provided as input, which in most cases is either difficult or inaccurate. The other drawback is that the nodalization along the longitude direction is very limited. Only one node at a time is simulated. For example, in the AFIP-1 test analysis (Section 8), a strip of fuel plate with a small length of 2.54 cm instead of a full length plate (54.6 cm) was simulated.

In the next version of DART-THEMAL, PLTEMP will replace the current 1-D thermal subroutine. PLTEMP is a FORTRAN program developed at ANL for obtaining a steady-state flow and temperature solution for a nuclear reactor core, or for a single fuel assembly [29]. PLTEMP has been used for calculation of temperatures in a reactor core loaded with flat fuel plates for the past 20 years. The temperature solution is effectively 2-dimensional. The fuel plates may be discretized into up to 5 layers in the thickness direction, and the width of a fuel plate can be divided into multiple longitudinal stripes. The temperature solution is repeated for each axial node along the length of the fuel assembly. This geometry nodalization scheme will allow DART-THERMAL to obtain fuel temperature information at any location in a fuel plate. Therefore, it will be possible to model fuel behavior at multiple locations in a fuel plate in a single run without setting up multiple cases in DART-THERMAL. This advantage will become more effective for simulating full-sized plates.

PLTEMP also provides a variety of thermal-hydraulic correlations, including the modified Dittus-Boelter equation (Eqn. (10.1)).

$$Nu_D = 0.023\,\mathrm{Re}_D^{\;0.8}\,\mathrm{Pr}^{0.4}\left(\frac{\mu_B}{\mu_S}\right)^{0.11} \tag{10.1}$$

where:
D is the inside diameter of the flow channel
Pr is the Prandtl number
μ_B is the fluid viscosity at the bulk fluid temperature
μ_S is the fluid viscosity at the heat-transfer boundary surface temperature

The classic Dittus-Boelter correlation (Eqn. (5.4)), implemented in the current version of DART-THERMAL, is explicit function for calculating the heat transfer coefficient between the bulk coolant and the fuel plate surface. It is easy to use, because it avoids equation complexity and iterative solution methodology. However, its application to a system with a large temperature difference across the fluid is less accurate. The modified Dittus-Boelter correlation is more accurate as it takes into account the change in viscosity due to temperature difference between the bulk coolant average temperature and the fuel plate surface temperature. The modified Dittus-Boelter correlation is solved by an iterative process, as the viscosity factor will change as the Nusselt number changes. After DART-THERMAL is updated with the 2-D PLTEMP thermal analysis subroutine, validation against experimental data will also be assessed.

The other DART-THERMAL improvement will be the introduction of a mechanism for the formation of large fission-gas-filled pores located at the IL-Al matrix and/or fuel particle-IL interfaces. Currently, fission-gas-bubbles are distributed randomly within the IL and do not aggregate at the interfaces between fuel particles and IL or the interfaces between IL and Al matrix, which is different from the microstructures observed in irradiated fuel plates. The absence of an appropriate fission-gas-bubble aggregation mechanism can result in underestimating of fuel meat swelling. In addition, the influence of these large pores on IL thermal conductivity is not accurately modeled. A constant value is currently used for IL thermal conductivity (Section 2.1). As such, including these large pores into the model will definitely increase the accuracy of DART-THERMAL in calculating fuel temperatures and fuel plate swelling.

References

[1] J. Rest, “The DART Dispersion Analysis Research Tool: A Mechanistic Model for Predicting Fission-Product-Induced Swelling of Aluminum Dispersion Fuels”, ANL-95/36, Argonne National Laboratory, 1995.

[2] J. Rest, G.L. Hofman, “DART Model for Irradiation-induced Swelling of Uranium Silicide Dispersion Fuel Elements”, Nuclear Technology, 126 (1999): 88-101.

[3] H. Taboada, R. Saliba, M. V. Moscarda, J. Rest, “Thermomechanical DART code improvements for LEU VHD Dispersion and Monolithic Fuel Element Analysis”, 26th RERTR meeting, Austria, 2004.

[4] J. Rest, and H. Taboada, “FASTDART- A Fast, Accurate and Friendly Version of DART code”, 22nd RERTR meeting, Las Vegas, USA, 2000.

[5] H. Taboada, J. Rest, M.V Moscarda, M. Markiewicz, and E. Estevez, “Development and Validation of An Improved Version of the DART code”, 24th RERTR meeting, Bariloche, Argentina, 2002.

[6] B. Ye, J. Rest, Argonne National Laboratory, private communication, 2012.

[7] B. Ye, Argonne National Laboratory, private communication, 2012.

[8] B. Ye, Argonne National Laboratory, private communication, 2013.

[9] J. Rest, Y.S. Kim, G.L. Hofman, M.K. Meyer, S.L. Hayes, “U-Mo Fuels Handbook”, ANL-09/31, Argonne National Laboratory, 2009.

[10] J. Rest, J.L. Snelgrove, and G.L. Hofman, “DART Model for Thermal Conductivity of U3Si2 Aluminum Dispersion Fuel”, 18th RERTR meeting, Paris, France, 1995.

[11] K.L. Peddicord, M.E. Cunningham and A. Tripathi, “Porosity correction to thermal Conductivity Based on Analytical Temperature Solutions”, Transaction of American Nuclear Society, 28 (1978): 548.

[12] J. Rest, G.L. Hofman, and Y.S. Kim, “Analysis of Intergranular Fission-gas Bubble-size Distributions in Irradiated Uranium-molybdenum Alloy Fuel”, Journal of Nuclear Materials, 385 (2009): 563-571.

[13] J. Rest, “Modeling of Fission-Gas-Induced Swelling of Nuclear Fuels”, In Comprehensive Nuclear Materials, ed. Rudy J.M. Konings, vol. 3, (Elsevier Science, 2012), 579-627.

[14] J. Rest, “GRASS-SST: A Comprehensive Mechanisitic Model for the Prediction of Fission-Gas Behavior in UO2 – Base Fuels during Steady-State and Transient Conditions”, NUREG/GR-2437 Vol. I, Argonne National Laboratory Report, ANL-78-53, 1978.

[15] D. Yun, J. Rest, A.M. Yacout, “Modeling of Fission-Gas Bubble Size Distribution in U-Mo Metal Alloys”, Proceeding of Global 2011, Makuhari, Japan, Dec. 11-16, 2011.

[16] R.C. Birtcher, S.E. Donnelly, and C. Templier, “Evolution of Helium Bubbles in Aluminum During Heavy-ion Irradiation”, Physical Review B., 50 (1994): 764-769.

[17] Y.S. Kim, G.L. Hofman, J.M. Park, H.J. Ryu, A.B. Robinson, D.M. Wachs, “Interdiffusion Layer Growth Correlations for U-Mo/Al-Si Dispersion Fuel During Irradiation”, 33rd RERTR meeting, Santiago, Chile, 2011.

[18] Y.S. Kim, G.L. Hofman, “Interdiffusion in U3Si-Al, U3Si2-Al, and USi-Al Dispersion Fuels during Irradiation”, Journal of Nuclear Materials, 410 (2011): 1-9.

[19] S.L. Hayes, M.K. Meyer, G.L. Hofman, and J.L. Snelgrove, “U-Mo/Al Dispersion Fuel Modeling”, 25th RERTR meeting, Chicago, USA, 2003.

[20] Chemical Engineer’s Handbook, R.H. Perry & C.H. Chilton McGraw-Hill Fifth edition.

[21] Y.S. Kim, G.L. Hofman, A.B. Robinson, J.L. Snelgrove, N. Hanan, “Oxidation of Aluminum Alloy Cladding for Research and Test Reactor Fuel”, Journal of nuclear Materials, 378 (2008): 220-228.

[22] J.C. Griess, H.C. Savage, J.L. English, ORNL-3541, Oak Ridge National Laboratory, 1964.

[23] Y.S. Kim, G.L. Hofman, J. Rest, and M.R. Finlay, Argonne National Laboratory, private communication, 2005.

[24] D.M. Wachs, D.E. Burkes, S.L. Hayes, and W. Skerjanc, “Modeling the Integrated Performance of Dispersion and Monolithic U-Mo Based Fuels”, 28th RERTR meeting, Cape Town, Republic of South Africa, 2006.

[25] D.M. Perez, M.A. Lillo, G.S. Chang, G.A. Roth, N.E. Woolstenhulme, D.M. Wachs, “AFIP-1 Irradiation Summary Report”, Idaho National Laboratory, 2011.

[26] Y.S. Kim, G.L. Hofman, M.R. Finlay, H.J. Ryu, “Volume fraction analysis of RERTR-6 and 7A plates”, Argonne National Laboratory, 2006.

[27] Y.S. Kim, G.L. Hofman, A.B. Robinson, J.L. Snelgrove, N. Hanan, “Oxidation of Aluminum Alloy Cladding for Research and Test Reactor Fuel”, Journal of Nuclear Materials, 378 (2008): 220-228.

[28] Y.S. Kim, G.L. Hofman, Argonne National Laboratory, private communication, 2012.

[29] A.P. Olson and M. Kalimullah, “A Users Guide to the PLTEMP/ANL V4.1 Code”, ANL/RERTR/TM-11-22, Argonne National Laboratory, 2011.

Appendix I. DART-THERMAL Input Description

A graphic input interface has been developed for DART-THERMAL. Users can define the input information by following the user-friendly input windows step by step, as shown in Figure I.1 (a)-(f), or by generating a valid input deck in a .txt file (shown in Table I.1) which will be read by the code. At each step of the input definition, the code runs data-proof checks.

Step 1: Build the input file either by modifying an existing or the most recently used file, or by defining a new data set.

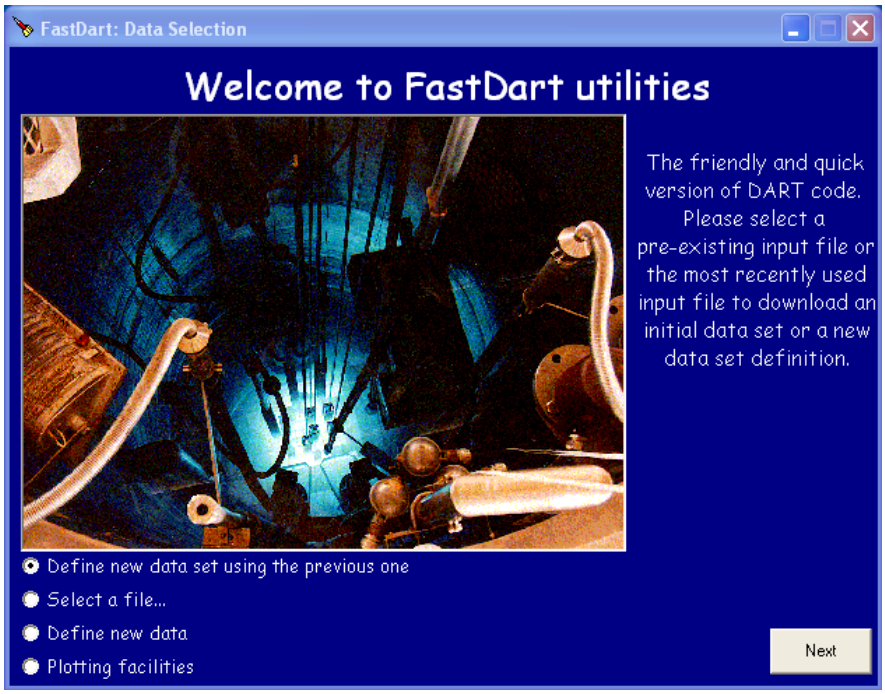

Figure I.1 (a) DART-THERMAL welcome window, where the user can choose from the options of building a new input file or modifying an existed file.

Information defined in step 1:

Appropriate option to build an input file.

Step 2: Define fuel geometry and dimensions, coolant properties, and oxide growth correlation

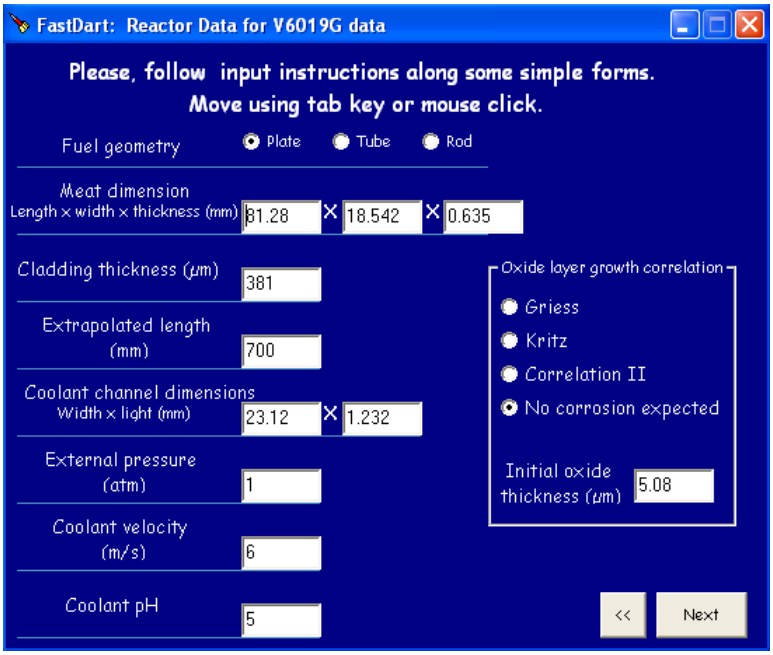

Figure I.1 (b) DART-THERMAL input window for definition of fuel geometry and dimensions, and coolant properties

Information defined in step 2:

Parameter	Unit
Fuel geometry	Plate, or tube, or rod
Fuel meat length	mm
Fuel meat width	mm
Fuel meat thickness	mm
Cladding thickness	µm
Extrapolated length (used for thermal calculation)	mm
Coolant channel width	mm
Coolant channel thickness	mm
External pressure	atm
Coolant velocity	m/s
Coolant pH value	No unit
Oxide growth correlation	Griess's, or Kritz's, or Correlation II, or No corrosion expected (this option in fact implemented with Kim's correlation)
Initial oxide thickness	µm

Step 3: Define fuel particle size distribution, initial constituent volume fractions in fuel meat, and fuel particle geometry and composition.

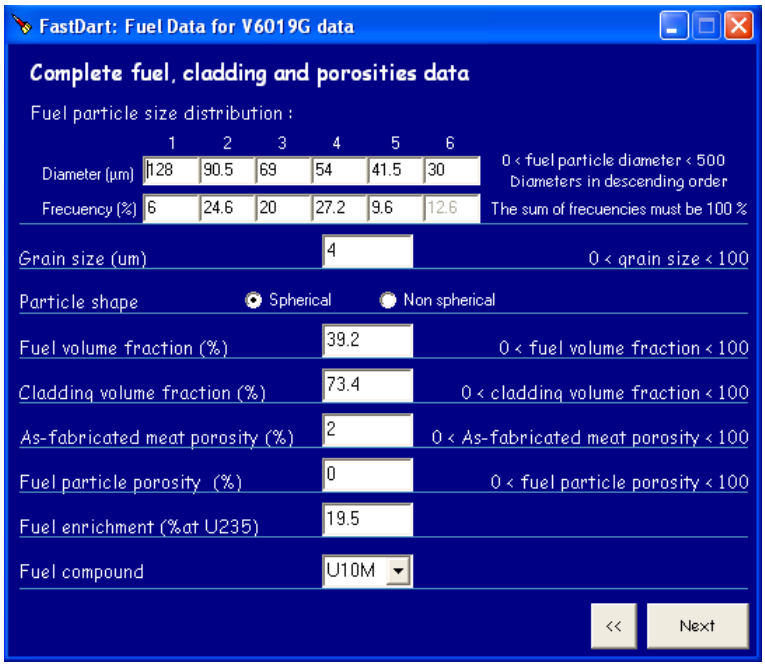

Figure I.1 (c) DART-THERMAL input window for definition of fuel particle distribution and initial fuel loading fractions

Information defined in step 3:

Parameter	Unit
Average diameter for each size group of fuel particles	µm
Frequency of each size group of fuel paticles	%
Fuel grain size (diameter)	µm
Fuel particle shape	spherical or non-spherical
Fuel/meat volume fraction	%
Cladding/fuel plate volume fraction	%
As-fabricated meat porosity	%
Fuel particle porosity	%
Fuel enrichment	^{235}U at%
Fuel compound type	U10Mo, or U6Mo, or U_3Si, or U_3Si_2

Step 4: Choose units for inputting reactor operation history

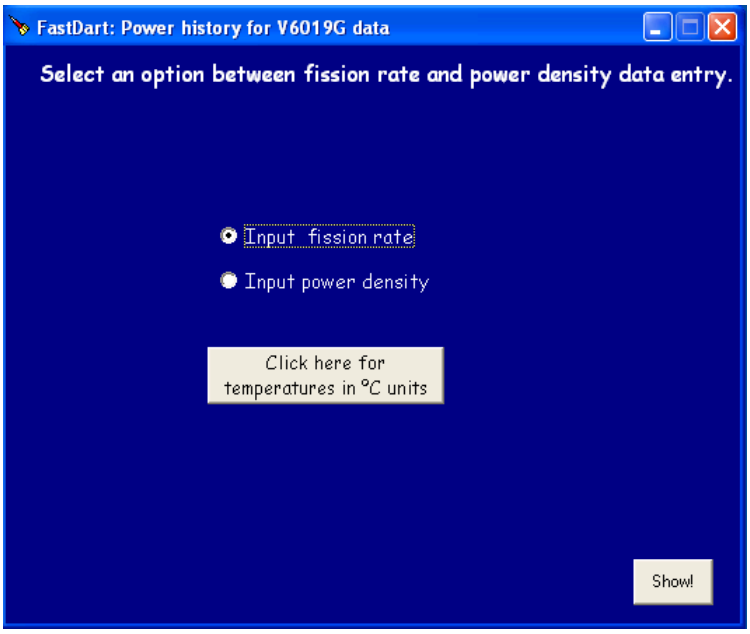

Figure I.1 (d) DART-THERMAL input window to choose units for power and temperature

Information defined in step 4:

Parameter	Options
Reactor operation power	Fission rate or power density
Temperature	K or °C

Step 5: Input operation history for a specific plate

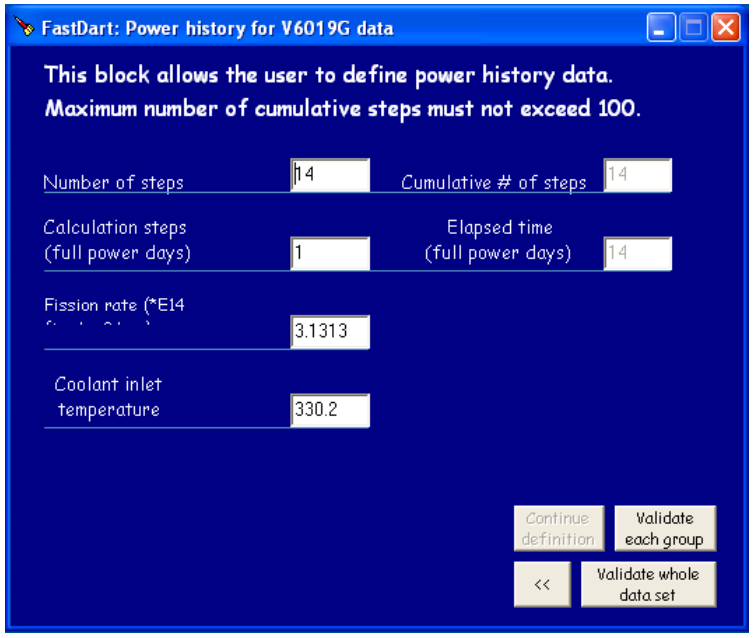

Figure I.1 (e) DART-THERMAL input window for power and coolant temperature at each time step

Information defined in step 5:

Parameter	Unit
Number of time step	No unit
Full power days per step	EFPD
Fission rate	10^{14} fissions/(cm^{3}s)
Coolant inlet temperature	K or °C
Cumulative time steps	No unit
Elapsed time	EFPD

Step 6: Choose Fastdart mode and run the calculation

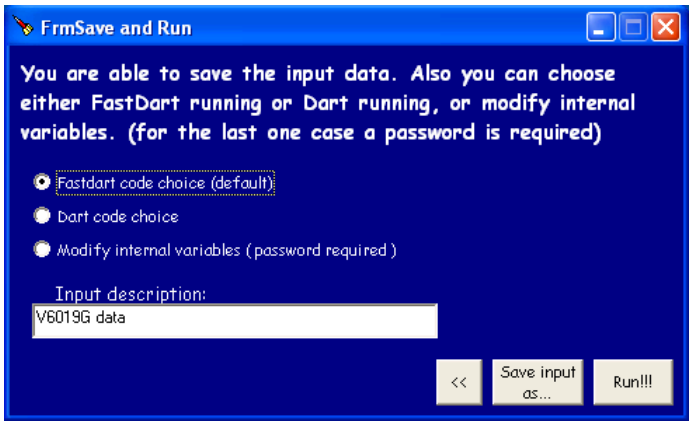

Figure I.1 (f) DART-THERMAL window for setting up the running mode

Table I.1 shows a sample input file for DART-THERMAL, where the user can also specify the parameters for each case, including the fuel geometry, dimensions, coolant properties, U-235 enrichment, initial constituent volume fractions, fuel particle size distribution, and fission rate and coolant temperature at each time step. It is worth to mention that the time step size is 1 EFPD, and the unit for fission rate is 10^{14} fissions/cm^3-s.

Table I.1 A sample input file for DART-THERMAL

Welcome to FastDart data input				
V6019G data				
Longitudinal partition length		0.1		
Geometry (0.5=plate/tube, 1=rod)		0.5		
Meat thickness (mm)		0.635		
Meat length (mm)(only plate)		81.28		
Meat width (mm)(only plate)		18.542		
Cladding thickness (µm)		381		
Extrapolated length (mm)		700		
Coolant channel width (mm)		23.12		
Coolant channel thickness (mm)		1.232		
Coolant velocity (m/s)		6		
Coolant pH		5		
External pressure (atm)		1		
Oxide layer growth correlation		None		
Initial oxide thickness (µm)		5.08		
Particle shape		spherical		
Grain particle diameter (µm)		4.0		
Fuel/meat vol fraccion (%)		39.2		
Cladding vol fraction (%)		73.40		
Meat fabrication porosity (%)		2		
Fuel particle porosity (%)		0		
U-235 enrichment (%)		19.5		
Fuel compound		U10Mo		
Gap gas pressure (atm)(only rod)		0		
1th fuel particle diameter (µm)		128.0		
2th fuel particle diameter (µm)		90.5		
3th fuel particle diameter (µm)		69.0		
4th fuel particle diameter (µm)		54.0		
5th fuel particle diameter (µm)		41.5		
6th fuel particle diameter (µm)		30.0		
1th radial particle frequency		6		
2th radial particle frequency		24.6		
3th radial particle frequency		20		
4th radial particle frequency		27.2		
5th radial particle frequency		9.6		
6th radial particle frequency		12.6		
Meat shape		Rectangular		
No. of steps	delti	Fission rate	Tinlet (K)	0
14	1	2.4640	325.2	0
14	1	2.3265	325.2	0
14	1	2.2691	325.2	0
5	1	2.6080	325.2	0
4	1	2.5298	325.2	0
4	1	2.4903	325.2	0

20	1	2.7715	325.2	0
19	1	2.5390	325.2	0
19	1	2.3346	325.2	0
0	0	0	0	0

Appendix II. DART-THERMAL Output Description

After each run, DART-THERMAL generates 11 output files. Table II.1 lists all output files and their contents. Among them, s.txt is the general output and contains all of the information generated during the calculation process. The complete description of each output parameter in s.txt can be found in [1]. Other output files store certain output information in a much simpler format in order to facilitate data processing.

Table II.2 DART-TERMAL output files

File name	Unit No.	Contents
output.csv	22	burnup, fuel meat swelling, constituent volume fractions, interaction layer thickness (cm), reacted fuel thickness in the largest fuel particle (cm), etc.
s.txt	lou	general output file containing all of the information
therm.csv	21	burnup, heat flux (W/cm^2), coolant-plate surface heat transfer coefficient (W/cm^2-K), coolant inlet temperature (°C), coolant outlet temperature (°C), coolant-oxidation layer interface temperature (°C), oxidation layer-cladding interface temperature (°C), cladding-fuel meat interface temperature (°C), fuel particle surface temperature (°C), fuel particle center temperature (°C)
zones.csv	18	meat zone number, fuel meat temperature (°C), fuel particle surface temperature (°C), fuel meat thermal conductivity (W/m-K), reacted fuel thickness in the largest fuel particle (µm), IL thickness (µm), and constituent volume fractions in each meat zone
DARTJinput.txt	19	time step (s), fission rate (fissions/cm^3-s), fuel meat temperature in the center zone (°C), fuel particle surface temperature in the center zone (°C)
test.csv	20	intermediate parameters for fuel-matrix interaction calculation
bulk.csv	15	intergranular bubble density in each size class (1/cm^3)
face.csv	16	intragranular bubble density in each size class (1/cm^3)
radbulk.csv	25	intergranular bubble radius of each size class (cm)
radface.csv	26	intragranular bubble radius of each size class (cm)
out.csv	12	irradiation time (EFPD), burnup, fission rate (fissions/cm^3-s), fission density (fissions/cm^3), constituent volume fractions, total meat swelling, IL thickness (µm), meat thermal conductivity (W/m-K), fuel thermal

conductivity (W/m-K), unreacted fuel swelling, IL swelling, swelling due to reaction

Appendix III. DART-THERMAL Installation Description

III.1 Files required to install DART-THERMAL

There is a detailed list of files (total 28 files) needed to install DART-THERMAL:

1. FastDart: five files: one executable file (.exe), two dynamic library links (.dll) for U3O8 or silicide option, and two input files:
FASTDART.EXE, FDART.DLL, FDINPUT.TXT, FDARTO.DLL, FDINPUT2.TXT

2. Fortran files: three .dll files:
DFORMD.DLL, DFORRT.DLL, and MSVCRT.DLL

3. Visual Basic 6.0: twenty files:
ASCTRLS.OCX, CMCT3ES.DLL, CMDLGES.DLL, COMCT332.OCX, COMDLG32.OCX, MSCC2ES.DLL, MSCH2ES.DLL, MSCHRT20.OCX, MSCMCES.DLL, MSCOMCT2.OCX, MSCOMCTL.OCX, MSSTDFMT.DLL, PLUGIN.OCX, MSVBVM60.DLL, SETUP.EXE, SETUP1.EXE, ST6UNST.EXE, STDFTES.DLL, VB6ES.DLL, VB6STKIT.DLL

III.2 DART-THERMAL installation instructions

The installation instructions described here indicate the specific version of software used for the calculations presented in this work. However, the same or similar procedures can be followed when the newer versions of the software are in use.

The installing program is Inno Setup version 1.3.26. It uses the fastdart.iss file. Once it is compiled and linked, the installation starts. The installer puts FastDart in the Program menu and drops the FastDart icon on the desktop. There must be a correspondence between the installation unit declared in fastdart.iss and the real (physical) place where the files are located. For instance, if the installation is to be performed from other source than c:\fastdart (i.e. a CD unit), the user must replace c letter for that associated with the CD unit.

DART and DART-THERMAL run on PC. Current operation of these codes is on Windows XP. DART and the calculation module in DART-THERMAL are written in FORTRAN 77 for the Lahey Fortran 95 compiler. The programs are compiled with Lahey Fortran 95 compiler for Windows PC. FORTRAN compilers from other companies, such as Intel and Compaq, can also be used, but extra attention will be required for minor differences in compilers. No nonstandard library routines are used in the codes.

DART-THERMAL is compiled as a Dynamic Library Link with Microsoft Developer Studio. This is the way to include the FORTRAN calculation subroutine into visual interfaces. The input data defined through the user interface (Figure I.1 (a)-(f)) are passed to the DLL as entry arrays. The calculation made by the DLL is returned as an export common block. The DLL can be compiled by following the processes below.

1. Run Microsoft Developer Studio
2. Choose **New** from the **File** manual
3. In the **Projects**, choose **Dynamic-Link Library**
4. Enter the Project name (eg. "fastdart") and the location (eg. "C:\fastdart\dll") to store the DLL
5. Add the FORTRAN subroutine (FDTHTDLL.FOR) into the newly defined project
6. Choose **Build** from the main manual
7. Choose the command of **Build fastdart.dll** from the **Build** submanual
8. When the command is executed, .opt, .dsw, .dsp, and .plg files and a "**Debug"** file folder will be created in the designated location (C:\fastdart\dll)
9. Copy the **"Debug"** folder into the location where DART-THERMAL is installed (eg. "C:\fastdart")
10. Run DART-THERMAL from the manual

If there are any modifications made to the FORTRAN module, it will be necessary to rebuild the DLL file. The rebuilding process will be from Step 6 to Step 10 to reflect the modification.

Nuclear Engineering Division
Argonne National Laboratory
9700 South Cass Avenue, Bldg. 208
Argonne, IL 60439-4842

www.anl.gov

Argonne National Laboratory is a U.S. Department of Energy
laboratory managed by UChicago Argonne, LLC